PHYSICAL REVIEW D **77,** 013008 (2008)

Survey of lepton number violation via effective operators

André de Gouvêa and James Jenkins

Northwestern University, Department of Physics & Astronomy, 2145 Sheridan Road, Evanston, Illinois 60208, USA

(Received 5 September 2007; published 30 January 2008)

We survey 129 lepton number violating effective operators, consistent with the minimal standard model gauge group and particle content, of mass dimension up to and including 11. Upon requiring that each one radiatively generates the observed neutrino masses, we extract an associated characteristic cutoff energy scale which we use to calculate other observable manifestations of these operators for a number of current and future experimental probes, concentrating on lepton number violating phenomena. These include searches for neutrinoless double-beta decay and rare meson, lepton, and gauge boson decays. We also consider searches at hadron/lepton collider facilities in anticipation of the CERN LHC and the future ILC. We find that some operators are already disfavored by current data, while more are ripe to be probed by next-generation experiments. We also find that our current understanding of lepton mixing disfavors a subset of higher dimensional operators. While neutrinoless double-beta decay is the most promising signature of lepton number violation for the majority of operators, a handful is best probed by other means. We argue that a combination of constraints from various independent experimental sources will help to pinpoint the ''correct'' model of neutrino mass, or at least aid in narrowing down the set of possibilities.

DOI: 10.1103/PhysRevD.77.013008 PACS numbers: 14.60.Pq

I. INTRODUCTION

The discovery of neutrino masses via their flavor oscillations over long baselines constitutes the first solid evidence of physics beyond the standard model (SM) of particle physics [1]. While this is an important first step toward a deeper understanding of nature, it poses many more questions than it answers. A number of theoretically well-motivated models have been proposed and explored to address the origin of the neutrino mass but, strictly speaking, these represent only a handful out of an infinite set of possibilities. The question of how well future experiments can probe and distinguish different scenarios arises naturally and is quite relevant given the current state of high-energy physics. The coming years promise detailed explorations of the Terascale with the CERN Large Hadron Collider (LHC) and the more distant International Linear Collider (ILC) or variants thereof. Expectations are that combined information from these two facilities, coupled with high-precision, low-energy results and cosmological observations, will shed light on some of the current mysteries of physics, including that of the neutrino mass.

Here, we concentrate on the possibility that the neutrino masses are generated at some high-energy scale Λ where $U(1)_{B-L}$, the only nonanomalous global symmetry of the standard model, is broken. Such a scenario is well motivated by the observed properties of the light neutrinos including tiny masses, large mixings, and the fact that neutrinos are the only electrically neutral fundamental fermions. More specifically, once $U(1)_{B-L}$ is broken, neutrinos are not protected from getting nonzero Majorana masses after electroweak symmetry breaking. On the other hand, since the renormalizable minimal standard model[1] preserves $U(1)_{B-L}$, $B-L$ breaking effects will only manifest themselves at low energies through higher dimensional operators. This being the case, one generically expects neutrino masses to be suppressed with respect to charged fermion masses by $(v/\Lambda)^n$, $n \geq 1$, where v is the Higgs boson vacuum expectation value (vev).

By further assuming that all new degrees of freedom are much heavier than the weak scale, we are guaranteed that, regardless of the details of the new physics sector, all phenomena below the weak scale are described by irrelevant, higher dimensional operators. In this spirit, the observable consequences of all high-energy models that lead to small Majorana neutrino masses can be catalogued by understanding the consequences of irrelevant operators that break $B-L$ by two units. With this in mind, we will survey all such nonrenormalizable effective operators for phenomenological signatures at future and current experiments. We restrict ourselves to operators that will lead to lepton number violation (LNV), as these will be directly connected to the existence of small Majorana neutrino masses. This means that we do not consider operators that conserve L but violate B, and hence also $B-L$, by two units (such operators lead to, for example, neutron-antineutron oscillations), nor do we include operators that respect $B-L$. Most of the time, the latter will not mediate

[1]Throughout, we will assume that the weak-scale degrees of freedom are the known standard model fields, plus a minimal Higgs sector. Hence, we assume that there are no gauge singlet ''right-handed neutrino'' fermions or higher $SU(2)_L$ Higgs boson representations, such as Higgs boson triplets.

any observable consequences for large enough Λ, except for operators of dimension six and above that can mediate proton decay.

To begin, we systematically name and classify all relevant LNV operators. Fortunately, this has already been done[2] in [2] up to and including operators of mass dimension 11.[3] For each operator we then calculate/estimate the analytic form of the radiatively generated neutrino-mass matrix. Upon setting this expression equal to the experimentally measured neutrino masses, we extract the energy scale Λ associated with the new LNV physics. Armed with these scales, we proceed to calculate each operator's phenomenological signatures at a variety of experimental settings. Additionally, having explicitly calculated the operator-induced neutrino-mass *matrices*, we may also verify, under some generic assumptions, whether one can account for the observable lepton mixing pattern. After such a general survey, one is adequately equipped to take a step back and select phenomenologically/theoretically interesting operators for further detailed study by ''expanding'' effective vertices to reveal particular ultraviolet completions. In this way, one can use the results presented here as a means of systematically generating renormalizable models with well-defined experimental predictions.

This paper is organized as follows. Section II is devoted to an introduction to the effective operators and methods. In the subsection of Sec. II, we derive and comment on the scales Λ of new physics that are used throughout the remainder of the text. In Sec. III, we survey various experimental probes of LNV for each operator, and address if and when our analysis breaks down due to added model structure or additional assumptions. Specifically, we study both current constraints and future prospects for neutrinoless double-beta-decay experiments in Sec. III A, followed, in Sec. III B, by a similar analysis of other rare decay modes, including those of various mesons and W/Z gauge bosons. In Sec. III C, we present collider signatures of LNV as they apply to future linear collider facilities running in the e^-e^- collision mode, and describe extensions of our analysis to include associated $\gamma\gamma$ collisions. We also comment on searches for LNV in future hadron machines. Section IV describes current constraints from neutrino oscillation phenomenology due to the general structure of the derived neutrino-mass matrices. In Sec. V, we highlight a number of ''interesting'' operators, defined by low cutoff scales and prominence of experimental signatures, which are still allowed by current constraints on LNV. We undertake a slightly more detailed discussion of their characteristics and signatures and present some sample ultraviolet completions. We conclude in Sec. VI with a summary of our assumptions and results, augmented by commentary on future prospects for LNV searches. Our results are tabulated by operator name in Table I for easy reference.

We hope that this analysis will prove useful to various audiences on a number of distinct levels. In the most superficial sense, the casual reader should note the general

TABLE I. Dimension-five through dimension-11 LNV operators analyzed in this survey. The first two columns display the operator name and field structure, respectively. Column three presents the induced neutrino-mass expressions, followed by the inferred scale of new physics, Λ_ν. Column five lists favorable modes of experimental exploration. Column six describes an operator's current status according to the key U (unconstrained), C (constrained), and D (disfavored). See text for details.

$\mathcal{O}$	Operator	$m_{\alpha\beta}$	Λ_ν(TeV)	Best probed	Disfavored
1	$L^iL^jH^kH^l\epsilon_{ik}\epsilon_{jl}$	$\frac{v^2}{\Lambda}$	6×10^{11}	$\beta\beta0\nu$	U
2	$L^iL^jL^ke^cH^l\epsilon_{ij}\epsilon_{kl}$	$\frac{y_e}{16\pi^2}\frac{v^2}{\Lambda}$	4×10^{7}	$\beta\beta0\nu$	U
3_a	$L^iL^jQ^kd^cH^l\epsilon_{ij}\epsilon_{kl}$	$\frac{y_dg^2}{(16\pi^2)^2}\frac{v^2}{\Lambda}$	2×10^{5}	$\beta\beta0\nu$	U
3_b	$L^iL^jQ^kd^cH^l\epsilon_{ik}\epsilon_{jl}$	$\frac{y_d}{16\pi^2}\frac{v^2}{\Lambda}$	1×10^{8}	$\beta\beta0\nu$	U
4_a	$L^iL^j\bar{Q}_i\bar{u}^cH^k\epsilon_{jk}$	$\frac{y_u}{16\pi^2}\frac{v^2}{\Lambda}$	4×10^{9}	$\beta\beta0\nu$	U
4_b	$L^iL^j\bar{Q}_k\bar{u}^cH^k\epsilon_{ij}$	$\frac{y_ug^2}{(16\pi^2)^2}\frac{v^2}{\Lambda}$	6×10^{6}	$\beta\beta0\nu$	U
5	$L^iL^jQ^kd^cH^lH^m\bar{H}_i\epsilon_{jl}\epsilon_{km}$	$\frac{y_d}{(16\pi^2)^2}\frac{v^2}{\Lambda}$	6×10^{5}	$\beta\beta0\nu$	U
6	$L^iL^j\bar{Q}_k\bar{u}^cH^lH^k\bar{H}_i\epsilon_{jl}$	$\frac{y_u}{(16\pi^2)^2}\frac{v^2}{\Lambda}$	2×10^{7}	$\beta\beta0\nu$	U

[2]The authors of [2] discuss all possible effective operators of dimensions up to and including 11, but only explicitly list those deemed unique in the sense that they cannot be written as the product of any previous operator with a standard model interaction. We append their list and naming scheme to include these into our analysis.

[3]We will argue later that irrelevant operators with mass dimension 13 and higher, if related to neutrino masses, will require new physics below the electroweak scale so that we would have already observed new physics if neutrino masses were generated in this way. Furthermore, from a model-building perspective, it is difficult to develop models that predominantly yield effective operators of very high mass dimension. The probability that such scenarios are both theoretically well motivated and evade all observations appears to be slim.

TABLE I. (*Continued*)

$\mathcal{O}$	Operator	$m_{\alpha\beta}$	Λ_ν(TeV)	Best probed	Disfavored
7	$L^i Q^j \bar{e}^c \bar{Q}_k H^k H^l H^m \epsilon_{il} \epsilon_{jm}$	$y_{\ell_\beta} \frac{g^2}{(16\pi^2)^2} \frac{v^2}{\Lambda} (\frac{1}{16\pi^2} + \frac{v^2}{\Lambda^2})$	4×10^2	mix	C
8	$L^i \bar{e}^c \bar{u}^c d^c H^j \epsilon_{ij}$	$y_{\ell_\beta} \frac{y_d y_u}{(16\pi^2)^2} \frac{v^2}{\Lambda}$	6×10^3	mix	C
9	$L^i L^j L^k e^c L^l e^c \epsilon_{ij} \epsilon_{kl}$	$\frac{y_\ell^2}{(16\pi^2)^2} \frac{v^2}{\Lambda}$	3×10^3	$\beta\beta 0\nu$	U
10	$L^i L^j L^k e^c Q^l d^c \epsilon_{ij} \epsilon_{kl}$	$\frac{y_\ell y_d}{(16\pi^2)^2} \frac{v^2}{\Lambda}$	6×10^3	$\beta\beta 0\nu$	U
11_a	$L^i L^j Q^k d^c Q^l d^c \epsilon_{ij} \epsilon_{kl}$	$\frac{y_d^2 g^2}{(16\pi^2)^3} \frac{v^2}{\Lambda}$	30	$\beta\beta 0\nu$	U
11_b	$L^i L^j Q^k d^c Q^l d^c \epsilon_{ik} \epsilon_{jl}$	$\frac{y_d^2}{(16\pi^2)^2} \frac{v^2}{\Lambda}$	2×10^4	$\beta\beta 0\nu$	U
12_a	$L^i L^j \bar{Q}_i \bar{u}^c \bar{Q}_j \bar{u}^c$	$\frac{y_u^2}{(16\pi^2)^2} \frac{v^2}{\Lambda}$	2×10^7	$\beta\beta 0\nu$	U
12_b	$L^i L^j \bar{Q}_k \bar{u}^c \bar{Q}_l \bar{u}^c \epsilon_{ij} \epsilon^{kl}$	$\frac{y_u^2 g^2}{(16\pi^2)^3} \frac{v^2}{\Lambda}$	4×10^4	$\beta\beta 0\nu$	U
13	$L^i L^j \bar{Q}_i \bar{u}^c L^l e^c \epsilon_{jl}$	$\frac{y_\ell y_u}{(16\pi^2)^2} \frac{v^2}{\Lambda}$	2×10^5	$\beta\beta 0\nu$	U
14_a	$L^i L^j \bar{Q}_k \bar{u}^c Q^k d^c \epsilon_{ij}$	$\frac{y_d y_u g^2}{(16\pi^2)^3} \frac{v^2}{\Lambda}$	1×10^3	$\beta\beta 0\nu$	U
14_b	$L^i L^j \bar{Q}_i \bar{u}^c Q^l d^c \epsilon_{jl}$	$\frac{y_d y_u}{(16\pi^2)^2} \frac{v^2}{\Lambda}$	6×10^5	$\beta\beta 0\nu$	U
15	$L^i L^j L^k d^c \bar{L}_i \bar{u}^c \epsilon_{jk}$	$\frac{y_d y_u g^2}{(16\pi^2)^3} \frac{v^2}{\Lambda}$	1×10^3	$\beta\beta 0\nu$	U
16	$L^i L^j e^c d^c \bar{e}^c \bar{u}^c \epsilon_{ij}$	$\frac{y_d y_u g^4}{(16\pi^2)^4} \frac{v^2}{\Lambda}$	2	$\beta\beta 0\nu$, LHC	U
17	$L^i L^j d^c d^c \bar{d}^c \bar{u}^c \epsilon_{ij}$	$\frac{y_d y_u g^4}{(16\pi^2)^4} \frac{v^2}{\Lambda}$	2	$\beta\beta 0\nu$, LHC	U
18	$L^i L^j d^c u^c \bar{u}^c \bar{u}^c \epsilon_{ij}$	$\frac{y_d y_u g^4}{(16\pi^2)^4} \frac{v^2}{\Lambda}$	2	$\beta\beta 0\nu$, LHC	U
18	$L^i Q^j d^c d^c \bar{e}^c \bar{u}^c \epsilon_{ij}$	$y_{\ell_\beta} \frac{y_d^2 y_u}{(16\pi^2)^3} \frac{v^2}{\Lambda}$	1	$\beta\beta 0\nu$, HElnv, LHC, mix	C
20	$L^i d^c \bar{Q}_i \bar{u}^c \bar{e}^c \bar{u}^c$	$y_{\ell_\beta} \frac{y_d y_u^2}{(16\pi^2)^3} \frac{v^2}{\Lambda}$	40	$\beta\beta 0\nu$, mix	C
21_a	$L^i L^j L^k e^c Q^l u^c H^m H^n \epsilon_{ij} \epsilon_{km} \epsilon_{ln}$	$\frac{y_\ell y_u}{(16\pi^2)^2} \frac{v^2}{\Lambda} (\frac{1}{16\pi^2} + \frac{v^2}{\Lambda^2})$	2×10^3	$\beta\beta 0\nu$	U
21_b	$L^i L^j L^k e^c Q^l u^c H^m H^n \epsilon_{il} \epsilon_{jm} \epsilon_{kn}$	$\frac{y_\ell y_u}{(16\pi^2)^2} \frac{v^2}{\Lambda} (\frac{1}{16\pi^2} + \frac{v^2}{\Lambda^2})$	2×10^3	$\beta\beta 0\nu$	U
22	$L^i L^j L^k e^c \bar{L}_k \bar{e}^c H^l H^m \epsilon_{il} \epsilon_{jm}$	$\frac{g^2}{(16\pi^2)^3} \frac{v^2}{\Lambda}$	4×10^4	$\beta\beta 0\nu$	U
23	$L^i L^j L^k e^c \bar{Q}_k \bar{d}^c H^l H^m \epsilon_{il} \epsilon_{jm}$	$\frac{y_\ell y_d}{(16\pi^2)^2} \frac{v^2}{\Lambda} (\frac{1}{16\pi^2} + \frac{v^2}{\Lambda^2})$	40	$\beta\beta 0\nu$	U
24_a	$L^i L^j Q^k d^c Q^l d^c H^m \bar{H}_i \epsilon_{jk} \epsilon_{lm}$	$\frac{y_d^2}{(16\pi^2)^3} \frac{v^2}{\Lambda}$	1×10^2	$\beta\beta 0\nu$	U
24_b	$L^i L^j Q^k d^c Q^l d^c H^m \bar{H}_i \epsilon_{jm} \epsilon_{kl}$	$\frac{y_d^2}{(16\pi^2)^3} \frac{v^2}{\Lambda}$	1×10^2	$\beta\beta 0\nu$	U
25	$L^i L^j Q^k d^c Q^l u^c H^m H^n \epsilon_{im} \epsilon_{jn} \epsilon_{kl}$	$\frac{y_d y_u}{(16\pi^2)^2} \frac{v^2}{\Lambda} (\frac{1}{16\pi^2} + \frac{v^2}{\Lambda^2})$	4×10^3	$\beta\beta 0\nu$	U
26_a	$L^i L^j Q^k d^c \bar{L}_i \bar{e}^c H^l H^m \epsilon_{jl} \epsilon_{km}$	$\frac{y_\ell y_d}{(16\pi^2)^3} \frac{v^2}{\Lambda}$	40	$\beta\beta 0\nu$	U
26_b	$L^i L^j Q^k d^c \bar{L}_k \bar{e}^c H^l H^m \epsilon_{il} \epsilon_{jm}$	$\frac{y_\ell y_d}{(16\pi^2)^2} \frac{v^2}{\Lambda} (\frac{1}{16\pi^2} + \frac{v^2}{\Lambda^2})$	40	$\beta\beta 0\nu$	U
27_a	$L^i L^j Q^k d^c \bar{Q}_i \bar{d}^c H^l H^m \epsilon_{jl} \epsilon_{km}$	$\frac{g^2}{(16\pi^2)^3} \frac{v^2}{\Lambda}$	4×10^4	$\beta\beta 0\nu$	U
27_b	$L^i L^j Q^k d^c \bar{Q}_k \bar{d}^c H^l H^m \epsilon_{il} \epsilon_{jm}$	$\frac{g^2}{(16\pi^2)^3} \frac{v^2}{\Lambda}$	4×10^4	$\beta\beta 0\nu$	U
28_a	$L^i L^j Q^k d^c \bar{Q}_j \bar{u}^c H^l \bar{H}_i \epsilon_{kl}$	$\frac{y_d y_u}{(16\pi^2)^3} \frac{v^2}{\Lambda}$	4×10^3	$\beta\beta 0\nu$	U
28_b	$L^i L^j Q^k d^c \bar{Q}_k \bar{u}^c H^l \bar{H}_i \epsilon_{jl}$	$\frac{y_d y_u}{(16\pi^2)^3} \frac{v^2}{\Lambda}$	4×10^3	$\beta\beta 0\nu$	U
28_c	$L^i L^j Q^k d^c \bar{Q}_l \bar{u}^c H^l \bar{H}_i \epsilon_{jk}$	$\frac{y_d y_u}{(16\pi^2)^3} \frac{v^2}{\Lambda}$	4×10^3	$\beta\beta 0\nu$	U
29_a	$L^i L^j Q^k u^c \bar{Q}_k \bar{u}^c H^l H^m \epsilon_{il} \epsilon_{jm}$	$\frac{y_u^2}{(16\pi^2)^2} \frac{v^2}{\Lambda} (\frac{1}{16\pi^2} + \frac{v^2}{\Lambda^2})$	2×10^5	$\beta\beta 0\nu$	U
29_b	$L^i L^j Q^k u^c \bar{Q}_l \bar{u}^c H^l H^m \epsilon_{ik} \epsilon_{jm}$	$\frac{g^2}{(16\pi^2)^3} \frac{v^2}{\Lambda}$	4×10^4	$\beta\beta 0\nu$	U
30_a	$L^i L^j \bar{L}_i \bar{e}^c \bar{Q}_k \bar{u}^c H^k H^l \epsilon_{jl}$	$\frac{y_\ell y_u}{(16\pi^2)^3} \frac{v^2}{\Lambda}$	2×10^3	$\beta\beta 0\nu$	U
30_b	$L^i L^j \bar{L}_m \bar{e}^c \bar{Q}_n \bar{u}^c H^k H^l \epsilon_{ik} \epsilon_{jl} \epsilon^{mn}$	$\frac{y_\ell y_u}{(16\pi^2)^2} \frac{v^2}{\Lambda} (\frac{1}{16\pi^2} + \frac{v^2}{\Lambda^2})$	2×10^3	$\beta\beta 0\nu$	U
31_a	$L^i L^j \bar{Q}_i \bar{d}^c \bar{Q}_k \bar{u}^c H^k H^l \epsilon_{jl}$	$\frac{y_d y_u}{(16\pi^2)^2} \frac{v^2}{\Lambda} (\frac{1}{16\pi^2} + \frac{v^2}{\Lambda^2})$	4×10^3	$\beta\beta 0\nu$	U
31_b	$L^i L^j \bar{Q}_m \bar{d}^c \bar{Q}_n \bar{u}^c H^k H^l \epsilon_{ik} \epsilon_{jl} \epsilon^{mn}$	$\frac{y_d y_u}{(16\pi^2)^2} \frac{v^2}{\Lambda} (\frac{1}{16\pi^2} + \frac{v^2}{\Lambda^2})$	4×10^3	$\beta\beta 0\nu$	U
32_a	$L^i L^j \bar{Q}_j \bar{u}^c \bar{Q}_k \bar{u}^c H^k \bar{H}_i$	$\frac{y_u^2}{(16\pi^2)^3} \frac{v^2}{\Lambda}$	2×10^5	$\beta\beta 0\nu$	U
32_b	$L^i L^j \bar{Q}_m \bar{u}^c \bar{Q}_n \bar{u}^c H^k \bar{H}_i \epsilon_{jk} \epsilon^{mn}$	$\frac{y_u^2}{(16\pi^2)^3} \frac{v^2}{\Lambda}$	2×10^5	$\beta\beta 0\nu$	U

TABLE I. (*Continued*)

$\mathcal{O}$	Operator	$m_{\alpha\beta}$	Λ_ν(TeV)	Best probed	Disfavored
33	$\bar{e}^c\bar{e}^c L^i L^j e^c e^c H^k H^l \epsilon_{ik}\epsilon_{jl}$	$\frac{g^2}{(16\pi^2)^3}\frac{v^2}{\Lambda}$	4×10^4	$\beta\beta0\nu$	U
34	$\bar{e}^c\bar{e}^c L^i Q^j e^c d^c H^k H^l \epsilon_{ik}\epsilon_{jl}$	$y_{\ell_\beta}\frac{y_d g^2}{(16\pi^2)^4}\frac{v^2}{\Lambda}$	<0.5	$\beta\beta0\nu$, mix, ILC, LHC	C
35	$\bar{e}^c\bar{e}^c L^i e^c \bar{Q}_j \bar{u}^c H^j H^k \epsilon_{ik}$	$y_{\ell_\beta}\frac{y_u g^2}{(16\pi^2)^4}\frac{v^2}{\Lambda}$	2	mix, LHC	C
36	$\bar{e}^c\bar{e}^c Q^i d^c Q^j d^c H^k H^l \epsilon_{ik}\epsilon_{jl}$	$y_{\ell_\alpha}y_{\ell_\beta}\frac{y_d^2 g^2}{(16\pi^2)^5}\frac{v^2}{\Lambda}$	<0.5	$\beta\beta0\nu$, mix, HElnv, ILC, LHC	D
37	$\bar{e}^c\bar{e}^c Q^i d^c \bar{Q}_j \bar{u}^c H^j H^k \epsilon_{ik}$	$y_{\ell_\alpha}y_{\ell_\beta}\frac{y_d y_u g^2}{(16\pi^2)^5}\frac{v^2}{\Lambda}$	<0.5	$\beta\beta0\nu$, mix, HElnv, ILC, LHC	D
38	$\bar{e}^c\bar{e}^c \bar{Q}_i \bar{u}^c \bar{Q}_j \bar{u}^c H^i H^j$	$y_{\ell_\alpha}y_{\ell_\beta}\frac{y_u^2 g^2}{(16\pi^2)^5}\frac{v^2}{\Lambda}$	<0.5	$\beta\beta0\nu$, mix, HElnv, ILC, LHC	D
39_a	$L^i L^j L^k L^l \bar{L}_i \bar{L}_j H^m H^n \epsilon_{km}\epsilon_{ln}$ [a]	$\frac{g^2}{(16\pi^2)^3}\frac{v^2}{\Lambda}$	8×10^4	$\beta\beta0\nu$	U
39_b	$L^i L^j L^k L^l \bar{L}_m \bar{L}_n H^m H^n \epsilon_{ij}\epsilon_{kl}$	$\frac{g^2}{(16\pi^2)^3}\frac{v^2}{\Lambda}$	4×10^4	$\beta\beta0\nu$	U
39_c	$L^i L^j L^k L^l \bar{L}_i \bar{L}_m H^m H^n \epsilon_{jk}\epsilon_{ln}$	$\frac{g^2}{(16\pi^2)^3}\frac{v^2}{\Lambda}$	4×10^4	$\beta\beta0\nu$	U
39_d	$L^i L^j L^k L^l \bar{L}_p \bar{L}_q H^m H^n \epsilon_{ij}\epsilon_{km}\epsilon_{ln}\epsilon^{pq}$	$\frac{g^2}{(16\pi^2)^3}\frac{v^2}{\Lambda}$	4×10^4	$\beta\beta0\nu$	U
40_a	$L^i L^j L^k Q^l \bar{L}_i \bar{Q}_j H^m H^n \epsilon_{km}\epsilon_{ln}$	$\frac{g^2}{(16\pi^2)^3}\frac{v^2}{\Lambda}$	4×10^4	$\beta\beta0\nu$	U
40_b	$L^i L^j L^k Q^l \bar{L}_i \bar{Q}_l H^m H^n \epsilon_{jm}\epsilon_{kn}$	$\frac{g^2}{(16\pi^2)^3}\frac{v^2}{\Lambda}$	4×10^4	$\beta\beta0\nu$	U
40_c	$L^i L^j L^k Q^l \bar{L}_l \bar{Q}_i H^m H^n \epsilon_{jm}\epsilon_{kn}$	$\frac{g^2}{(16\pi^2)^3}\frac{v^2}{\Lambda}$	4×10^4	$\beta\beta0\nu$	U
40_d	$L^i L^j L^k Q^l \bar{L}_i \bar{Q}_m H^m H^n \epsilon_{jk}\epsilon_{ln}$	$\frac{g^2}{(16\pi^2)^3}\frac{v^2}{\Lambda}$	4×10^4	$\beta\beta0\nu$	U
40_e	$L^i L^j L^k Q^l \bar{L}_i \bar{Q}_m H^m H^n \epsilon_{jl}\epsilon_{kn}$	$\frac{g^2}{(16\pi^2)^3}\frac{v^2}{\Lambda}$	4×10^4	$\beta\beta0\nu$	U
40_f	$L^i L^j L^k Q^l \bar{L}_m \bar{Q}_i H^m H^n \epsilon_{jk}\epsilon_{ln}$	$\frac{g^2}{(16\pi^2)^3}\frac{v^2}{\Lambda}$	4×10^4	$\beta\beta0\nu$	U
40_g	$L^i L^j L^k Q^l \bar{L}_m \bar{Q}_i H^m H^n \epsilon_{jl}\epsilon_{kn}$	$\frac{g^2}{(16\pi^2)^3}\frac{v^2}{\Lambda}$	4×10^4	$\beta\beta0\nu$	U
40_h	$L^i L^j L^k Q^l \bar{L}_m \bar{Q}_n H^m H^n \epsilon_{ij}\epsilon_{kl}$	$\frac{g^2}{(16\pi^2)^3}\frac{v^2}{\Lambda}$	4×10^4	$\beta\beta0\nu$	U
40_i	$L^i L^j L^k Q^l \bar{L}_m \bar{Q}_n H^p H^q \epsilon_{ip}\epsilon_{jq}\epsilon_{kl}\epsilon^{mn}$	$\frac{g^2}{(16\pi^2)^3}\frac{v^2}{\Lambda}$	4×10^4	$\beta\beta0\nu$	U
40_j	$L^i L^j L^k Q^l \bar{L}_m \bar{Q}_n H^p H^q \epsilon_{ip}\epsilon_{lq}\epsilon_{jk}\epsilon^{mn}$	$\frac{g^2}{(16\pi^2)^3}\frac{v^2}{\Lambda}$	4×10^4	$\beta\beta0\nu$	U
41_a	$L^i L^j L^k d^c \bar{L}_i \bar{d}^c H^l H^m \epsilon_{jl}\epsilon_{km}$	$\frac{g^2}{(16\pi^2)^3}\frac{v^2}{\Lambda}$	4×10^4	$\beta\beta0\nu$	U
41_b	$L^i L^j L^k d^c \bar{L}_l \bar{d}^c H^l H^m \epsilon_{ij}\epsilon_{km}$	$\frac{g^2}{(16\pi^2)^3}\frac{v^2}{\Lambda}$	4×10^4	$\beta\beta0\nu$	U
42_a	$L^i L^j L^k u^c \bar{L}_i \bar{u}^c H^l H^m \epsilon_{jl}\epsilon_{km}$	$\frac{g^2}{(16\pi^2)^3}\frac{v^2}{\Lambda}$	4×10^4	$\beta\beta0\nu$	U
42_b	$L^i L^j L^k u^c \bar{L}_l \bar{u}^c H^l H^m \epsilon_{ij}\epsilon_{km}$	$\frac{g^2}{(16\pi^2)^3}\frac{v^2}{\Lambda}$	4×10^4	$\beta\beta0\nu$	U
43_a	$L^i L^j L^k d^c \bar{L}_l \bar{u}^c H^l \bar{H}_i \epsilon_{jk}$	$\frac{y_d y_u g^2}{(16\pi^2)^4}\frac{v^2}{\Lambda}$	6	$\beta\beta0\nu$, LHC	U
43_b	$L^i L^j L^k d^c \bar{L}_j \bar{u}^c H^l \bar{H}_i \epsilon_{kl}$	$\frac{y_d y_u g^2}{(16\pi^2)^4}\frac{v^2}{\Lambda}$	6	$\beta\beta0\nu$, LHC	U
43_c	$L^i L^j L^k d^c \bar{L}_l \bar{u}^c H^m \bar{H}_n \epsilon_{ij}\epsilon_{km}\epsilon^{ln}$	$\frac{y_d y_u g^2}{(16\pi^2)^4}\frac{v^2}{\Lambda}$	6	$\beta\beta0\nu$, LHC	U
44_a	$L^i L^j Q^k e^c \bar{Q}_i \bar{e}^c H^l H^m \epsilon_{jl}\epsilon_{km}$	$\frac{g^2}{(16\pi^2)^3}\frac{v^2}{\Lambda}$	4×10^4	$\beta\beta0\nu$	U
44_b	$L^i L^j Q^k e^c \bar{Q}_k \bar{e}^c H^l H^m \epsilon_{il}\epsilon_{jm}$	$\frac{g^2}{(16\pi^2)^3}\frac{v^2}{\Lambda}$	4×10^4	$\beta\beta0\nu$	U
44_c	$L^i L^j Q^k e^c \bar{Q}_l \bar{e}^c H^l H^m \epsilon_{ij}\epsilon_{km}$	$\frac{g^4}{(16\pi^2)^4}\frac{v^2}{\Lambda}$	60	$\beta\beta0\nu$	U
44_d	$L^i L^j Q^k e^c \bar{Q}_l \bar{e}^c H^l H^m \epsilon_{ik}\epsilon_{jm}$	$\frac{g^2}{(16\pi^2)^3}\frac{v^2}{\Lambda}$	4×10^4	$\beta\beta0\nu$	U
45	$L^i L^j e^c d^c \bar{e}^c \bar{d}^c H^k H^l \epsilon_{ik}\epsilon_{jl}$	$\frac{g^2}{(16\pi^2)^3}\frac{v^2}{\Lambda}$	4×10^4	$\beta\beta0\nu$	U
46	$L^i L^j e^c u^c \bar{e}^c \bar{u}^c H^k H^l \epsilon_{ik}\epsilon_{jl}$	$\frac{g^2}{(16\pi^2)^3}\frac{v^2}{\Lambda}$	4×10^4	$\beta\beta0\nu$	U
47_a	$L^i L^j Q^k Q^l \bar{Q}_i \bar{Q}_j H^m H^n \epsilon_{km}\epsilon_{ln}$	$\frac{g^2}{(16\pi^2)^3}\frac{v^2}{\Lambda}$	4×10^4	$\beta\beta0\nu$	U
47_b	$L^i L^j Q^k Q^l \bar{Q}_i \bar{Q}_k H^m H^n \epsilon_{jm}\epsilon_{ln}$	$\frac{g^2}{(16\pi^2)^3}\frac{v^2}{\Lambda}$	4×10^4	$\beta\beta0\nu$	U
47_c	$L^i L^j Q^k Q^l \bar{Q}_k \bar{Q}_l H^m H^n \epsilon_{im}\epsilon_{jn}$	$\frac{g^2}{(16\pi^2)^3}\frac{v^2}{\Lambda}$	4×10^4	$\beta\beta0\nu$	U
47_d	$L^i L^j Q^k Q^l \bar{Q}_i \bar{Q}_m H^m H^n \epsilon_{jk}\epsilon_{ln}$	$\frac{g^2}{(16\pi^2)^3}\frac{v^2}{\Lambda}$	4×10^4	$\beta\beta0\nu$	U
47_e	$L^i L^j Q^k Q^l \bar{Q}_i \bar{Q}_m H^m H^n \epsilon_{jn}\epsilon_{kl}$	$\frac{g^2}{(16\pi^2)^3}\frac{v^2}{\Lambda}$	4×10^4	$\beta\beta0\nu$	U
47_f	$L^i L^j Q^k Q^l \bar{Q}_k \bar{Q}_m H^m H^n \epsilon_{ij}\epsilon_{ln}$	$\frac{g^4}{(16\pi^2)^4}\frac{v^2}{\Lambda}$	60	$\beta\beta0\nu$	U

TABLE I. (*Continued*)

$\mathcal{O}$	Operator	$m_{\alpha\beta}$	Λ_ν(TeV)	Best probed	Disfavored
47_g	$L^iL^jQ^kQ^l\bar{Q}_k\bar{Q}_mH^mH^n\epsilon_{il}\epsilon_{jn}$	$\frac{g^2}{(16\pi^2)^3}\frac{v^2}{\Lambda}$	4×10^4	$\beta\beta0\nu$	U
47_h	$L^iL^jQ^kQ^l\bar{Q}_p\bar{Q}_qH^mH^n\epsilon_{ij}\epsilon_{km}\epsilon_{ln}\epsilon^{pq}$	$\frac{g^4}{(16\pi^2)^4}\frac{v^2}{\Lambda}$	60	$\beta\beta0\nu$	U
47_i	$L^iL^jQ^kQ^l\bar{Q}_p\bar{Q}_qH^mH^n\epsilon_{ik}\epsilon_{jm}\epsilon_{ln}\epsilon^{pq}$	$\frac{g^2}{(16\pi^2)^3}\frac{v^2}{\Lambda}$	4×10^4	$\beta\beta0\nu$	U
47_j	$L^iL^jQ^kQ^l\bar{Q}_p\bar{Q}_qH^mH^n\epsilon_{im}\epsilon_{jn}\epsilon_{kl}\epsilon^{pq}$	$\frac{g^2}{(16\pi^2)^3}\frac{v^2}{\Lambda}$	4×10^4	$\beta\beta0\nu$	U
48	$L^iL^jd^cd^c\bar{d}^c\bar{d}^cH^kH^l\epsilon_{ik}\epsilon_{jl}$	$\frac{g^2}{(16\pi^2)^3}\frac{v^2}{\Lambda}$	4×10^4	$\beta\beta0\nu$	U
49	$L^iL^jd^cu^c\bar{d}^c\bar{u}^cH^kH^l\epsilon_{ik}\epsilon_{jl}$	$\frac{g^2}{(16\pi^2)^3}\frac{v^2}{\Lambda}$	4×10^4	$\beta\beta0\nu$	U
50	$L^iL^jd^cd^c\bar{d}^c\bar{u}^cH^k\bar{H}_i\epsilon_{jk}$	$\frac{y_dy_ug^2}{(16\pi^2)^4}\frac{v^2}{\Lambda}$	6	$\beta\beta0\nu$ LHC	U
51	$L^iL^ju^cu^c\bar{u}^c\bar{u}^cH^kH^l\epsilon_{ik}\epsilon_{jl}$	$\frac{g^2}{(16\pi^2)^3}\frac{v^2}{\Lambda}$	4×10^4	$\beta\beta0\nu$	U
52	$L^iL^jd^cu^c\bar{u}^c\bar{u}^cH^k\bar{H}_i\epsilon_{jk}$	$\frac{y_dy_ug^2}{(16\pi^2)^4}\frac{v^2}{\Lambda}$	6	$\beta\beta0\nu$, LHC	U
53	$L^iL^jd^cd^c\bar{u}^c\bar{u}^c\bar{H}_i\bar{H}_j$	$\frac{y_d^2y_u^2g^2}{(16\pi^2)^5}\frac{v^2}{\Lambda}$	<0.5	$\beta\beta0\nu$, HElnv, ILC, LHC	D
54_a	$L^iQ^jQ^kd^c\bar{Q}_i\bar{e}^cH^lH^m\epsilon_{jl}\epsilon_{km}$	$y_{\ell_\beta}\frac{y_dg^2}{(16\pi^2)^4}\frac{v^2}{\Lambda}$	<0.5	$\beta\beta0\nu$, mix, HElnv, ILC, LHC	D
54_b	$L^iQ^jQ^kd^c\bar{Q}_j\bar{e}^cH^lH^m\epsilon_{il}\epsilon_{km}$	$y_{\ell_\beta}\frac{y_dg^2}{(16\pi^2)^4}\frac{v^2}{\Lambda}$	<0.5	$\beta\beta0\nu$, mix, HElnv, ILC, LHC	D
54_c	$L^iQ^jQ^kd^c\bar{Q}_l\bar{e}^cH^lH^m\epsilon_{im}\epsilon_{jk}$	$y_{\ell_\beta}\frac{y_dg^2}{(16\pi^2)^4}\frac{v^2}{\Lambda}$	<0.5	$\beta\beta0\nu$, mix, ILC, LHC	D
54_d	$L^iQ^jQ^kd^c\bar{Q}_l\bar{e}^cH^lH^m\epsilon_{ij}\epsilon_{km}$	$y_{\ell_\beta}\frac{y_dg^2}{(16\pi^2)^4}\frac{v^2}{\Lambda}$	<0.5	$\beta\beta0\nu$,mix, HElnv, ILC, LHC	D
55_a	$L^iQ^j\bar{Q}_i\bar{Q}_k\bar{e}^c\bar{u}^cH^kH^l\epsilon_{jl}$	$y_{\ell_\beta}\frac{y_ug^2}{(16\pi^2)^4}\frac{v^2}{\Lambda}$	2	$\beta\beta0\nu$, mix, LHC	C
55_b	$L^iQ^j\bar{Q}_j\bar{Q}_k\bar{e}^c\bar{u}^cH^kH^l\epsilon_{il}$	$y_{\ell_\beta}\frac{y_ug^2}{(16\pi^2)^4}\frac{v^2}{\Lambda}$	2	$\beta\beta0\nu$, mix, LHC	C
55_c	$L^iQ^j\bar{Q}_m\bar{Q}_n\bar{e}^c\bar{u}^cH^kH^l\epsilon_{ik}\epsilon_{jl}\epsilon^{mn}$	$y_{\ell_\beta}\frac{y_ug^2}{(16\pi^2)^4}\frac{v^2}{\Lambda}$	2	$\beta\beta0\nu$, mix, LHC	C
56	$L^iQ^jd^cd^c\bar{e}^c\bar{d}^cH^kH^l\epsilon_{ik}\epsilon_{jl}$	$y_{\ell_\beta}\frac{y_dg^2}{(16\pi^2)^4}\frac{v^2}{\Lambda}$	<0.5	$\beta\beta0\nu$, mix, ILC, LHC	C
57	$L^id^c\bar{Q}_j\bar{u}^c\bar{e}^c\bar{d}^cH^jH^k\epsilon_{ik}$	$y_{\ell_\beta}\frac{y_ug^2}{(16\pi^2)^4}\frac{v^2}{\Lambda}$	2	$\beta\beta0\nu$, mix, LHC	C
58	$L^iu^c\bar{Q}_j\bar{u}^c\bar{e}^c\bar{u}^cH^jH^k\epsilon_{ik}$	$y_{\ell_\beta}\frac{y_ug^2}{(16\pi^2)^4}\frac{v^2}{\Lambda}$	2	mix, LHC	C
59	$L^iQ^jd^cd^c\bar{e}^c\bar{u}^cH^k\bar{H}_i\epsilon_{jk}$	$y_{\ell_\beta}\frac{y_d^2y_u}{(16\pi^2)^4}\frac{v^2}{\Lambda}$	<0.5	$\beta\beta0\nu$, mix, HElnv, ILC, LHC	D
60	$L^id^c\bar{Q}_j\bar{u}^c\bar{e}^c\bar{u}^cH^j\bar{H}_i$	$y_{\ell_\beta}\frac{y_dy_u^2}{(16\pi^2)^4}\frac{v^2}{\Lambda}$	<0.5	$\beta\beta0\nu$, mix, HElnv, ILC, LHC	D
61	$L^iL^jH^kH^lL^re^c\bar{H}_r\epsilon_{ik}\epsilon_{jl}$	$\frac{y_\ell}{16\pi^2}\frac{v^2}{\Lambda}(\frac{1}{16\pi^2}+\frac{v^2}{\Lambda^2})$	2×10^5	$\beta\beta0\nu$	U
62	$L^iL^jL^ke^cH^lL^re^c\bar{H}_r\epsilon_{ij}\epsilon_{kl}$	$\frac{y_\ell^2}{(16\pi^2)^2}\frac{v^2}{\Lambda}(\frac{1}{16\pi^2}+\frac{v^2}{\Lambda^2})$	20	$\beta\beta0\nu$	U
63_a	$L^iL^jQ^kd^cH^lL^re^c\bar{H}_r\epsilon_{ij}\epsilon_{kl}$	$\frac{y_\ell y_d}{(16\pi^2)^3}\frac{v^2}{\Lambda}$	40	$\beta\beta0\nu$	U
63_b	$L^iL^jQ^kd^cH^lL^re^c\bar{H}_r\epsilon_{ik}\epsilon_{jl}$	$\frac{y_\ell y_d}{(16\pi^2)^2}\frac{v^2}{\Lambda}(\frac{1}{16\pi^2}+\frac{v^2}{\Lambda^2})$	40	$\beta\beta0\nu$	U
64_a	$L^iL^j\bar{Q}_i\bar{u}^cH^kL^re^c\bar{H}_r\epsilon_{jk}$	$\frac{y_\ell y_u}{(16\pi^2)^2}\frac{v^2}{\Lambda}(\frac{1}{16\pi^2}+\frac{v^2}{\Lambda^2})$	2×10^3	$\beta\beta0\nu$	U
64_b	$L^iL^j\bar{Q}_k\bar{u}^cH^kL^re^c\bar{H}_r\epsilon_{ij}$	$\frac{y_\ell y_u}{(16\pi^2)^3}\frac{v^2}{\Lambda}$	2×10^3	$\beta\beta0\nu$	U
65	$L^i\bar{e}^c\bar{u}^cd^cH^jL^re^c\bar{H}_r\epsilon_{ij}$	$\frac{y_dy_ug^2}{(16\pi^2)^4}\frac{v^2}{\Lambda}$	6	$\beta\beta0\nu$, LHC	U
66	$L^iL^jH^kH^l\epsilon_{ik}Q^rd^c\bar{H}_r\epsilon_{jl}$	$\frac{y_d}{16\pi^2}\frac{v^2}{\Lambda}(\frac{1}{16\pi^2}+\frac{v^2}{\Lambda^2})$	6×10^5	$\beta\beta0\nu$	U
67	$L^iL^jL^ke^cH^lQ^rd^c\bar{H}_r\epsilon_{ij}\epsilon_{kl}$	$\frac{y_\ell y_d}{(16\pi^2)^2}\frac{v^2}{\Lambda}(\frac{1}{16\pi^2}+\frac{v^2}{\Lambda^2})$	40	$\beta\beta0\nu$	U
68_a	$L^iL^jQ^kd^cH^lQ^rd^c\bar{H}_r\epsilon_{ij}\epsilon_{kl}$	$\frac{y_d^2g^2}{(16\pi^2)^3}\frac{v^2}{\Lambda}(\frac{1}{16\pi^2}+\frac{v^2}{\Lambda^2})$	1	$\beta\beta0\nu$, LHC	U
68_b	$L^iL^jQ^kd^cH^lQ^rd^c\bar{H}_r\epsilon_{ik}\epsilon_{jl}$	$\frac{y_d^2}{(16\pi^2)^2}\frac{v^2}{\Lambda}(\frac{1}{16\pi^2}+\frac{v^2}{\Lambda^2})$	1×10^2	$\beta\beta0\nu$	U
69_a	$L^iL^j\bar{Q}_i\bar{u}^cH^kQ^rd^c\bar{H}_r\epsilon_{jk}$	$\frac{y_dy_u}{(16\pi^2)^2}\frac{v^2}{\Lambda}(\frac{1}{16\pi^2}+\frac{v^2}{\Lambda^2})$	4×10^3	$\beta\beta0\nu$	U
69_b	$L^iL^j\bar{Q}_k\bar{u}^cH^kQ^rd^c\bar{H}_r\epsilon_{ij}$	$\frac{y_dy_ug^2}{(16\pi^2)^3}\frac{v^2}{\Lambda}(\frac{1}{16\pi^2}+\frac{v^2}{\Lambda^2})$	7	$\beta\beta0\nu$, LHC	U
70	$L^i\bar{e}^c\bar{u}^cd^cH^jQ^rd^c\bar{H}_r\epsilon_{ij}$	$y_{\ell_\beta}\frac{y_d^2y_u}{(16\pi^2)^3}\frac{v^2}{\Lambda}(\frac{1}{16\pi^2}+\frac{v^2}{\Lambda^2})$	<0.5	$\beta\beta0\nu$, mix, HElnv, ILC, LHC	D
71	$L^iL^jH^kH^lQ^ru^cH^s\epsilon_{rs}\epsilon_{ik}\epsilon_{jl}$	$\frac{y_u}{16\pi^2}\frac{v^2}{\Lambda}(\frac{1}{16\pi^2}+\frac{v^2}{\Lambda^2})$	2×10^7	$\beta\beta0\nu$	U
72	$L^iL^jL^ke^cH^lQ^ru^cH^s\epsilon_{rs}\epsilon_{ij}\epsilon_{kl}$	$\frac{y_\ell y_u}{(16\pi^2)^2}\frac{v^2}{\Lambda}(\frac{1}{16\pi^2}+\frac{v^2}{\Lambda^2})$	2×10^3	$\beta\beta0\nu$	U
73_a	$L^iL^jQ^kd^cH^lQ^ru^cH^s\epsilon_{rs}\epsilon_{ij}\epsilon_{kl}$	$\frac{y_dy_ug^2}{(16\pi^2)^3}\frac{v^2}{\Lambda}(\frac{1}{16\pi^2}+\frac{v^2}{\Lambda^2})$	7	$\beta\beta0\nu$, LHC	U

TABLE I. (*Continued*)

$\mathcal{O}$	Operator	$m_{\alpha\beta}$	Λ_ν(TeV)	Best probed	Disfavored
73_b	$L^iL^jQ^kd^cH^lQ^ru^cH^s\epsilon_{rs}\epsilon_{ik}\epsilon_{jl}$	$\frac{y_dy_u}{(16\pi^2)^2}\frac{v^2}{\Lambda}(\frac{1}{16\pi^2}+\frac{v^2}{\Lambda^2})$	4×10^3	$\beta\beta0\nu$	U
74_a	$L^iL^j\bar{Q}_i\bar{u}^cH^kQ^ru^cH^s\epsilon_{rs}\epsilon_{jk}$	$\frac{y_u^2}{(16\pi^2)^2}\frac{v^2}{\Lambda}(\frac{1}{16\pi^2}+\frac{v^2}{\Lambda^2})$	2×10^5	$\beta\beta0\nu$	U
74_b	$L^iL^j\bar{Q}_k\bar{u}^cH^kQ^ru^cH^s\epsilon_{rs}\epsilon_{ij}$	$\frac{y_u^2g^2}{(16\pi^2)^3}\frac{v^2}{\Lambda}(\frac{1}{16\pi^2}+\frac{v^2}{\Lambda^2})$	2×10^2	$\beta\beta0\nu$	U
75	$L^i\bar{e}^c\bar{u}^cd^cH^jQ^ru^cH^s\epsilon_{rs}\epsilon_{ij}$	$y_{\ell_\beta}\frac{y_dy_u^2}{(16\pi^2)^3}\frac{v^2}{\Lambda}(\frac{1}{16\pi^2}+\frac{v^2}{\Lambda^2})$	1	$\beta\beta0\nu$, mix	C

[a]This operator is modified slightly from its original form as given in Ref. [2] where it appeared as $\mathcal{O}_{39}(a) = L^iL^jL^kL^l\bar{L}_i\bar{L}_jH^mH^n\epsilon_{jm}\epsilon_{kl}$. We corrected this error.

features of LNV as well as the diversity of model variations. Such information is best expressed in terms of the operator distribution histograms scattered throughout the text. These are color-coded by operator dimension or cutoff scale, and typically contain additional information, including current experimental prospects. On the more technical side, those interested in specific neutrino-mass generating models will find detailed, operator-specific information that may be utilized as crude model predictions. Additionally, as already alluded to, one may even ''hand-pick'' operators for model development based on specific phenomenological criteria. Finally, we urge experimentalists to search for new physics in all accessible channels. It is our ultimate goal to provide motivation for experimental considerations of nonstandard LNV effects, beyond neutrinoless double-beta decay.

II. THE LEPTON NUMBER VIOLATING SCALE

Here we analyze $SU(3)_c \times SU(2)_L \times U(1)_Y$ invariant $\Delta L = 2$ nonrenormalizable effective operators of mass dimension up to and including 11. They are composed of only the SM field content as all other, presumably heavy, degrees of freedom are integrated out. As already emphasized, we do not allow for the existence of SM singlet states (right-handed neutrinos) or any other ''enablers'' of renormalizable neutrino masses, such as Higgs $SU(2)_L$ triplet states. We therefore assume that all lepton number violation originates from new ultraviolet physics and that neutrino masses are generated at some order in perturbation theory.

A d-dimensional operator $\mathcal{O}^d$ is suppressed by $d-4$ powers of a mass scale Λ that characterizes the new physics, in addition to a dimensionless coupling constant λ:

$$\mathcal{L} \in \sum_i \frac{\lambda_i \mathcal{O}_i^d}{\Lambda^{d-4}}, \tag{2.1}$$

where we sum over all possible flavor combinations that make up the same ''operator-type,'' as defined below. For each operator, Λ/λ is approximately the maximum energy scale below which the new perturbative ultraviolet physics is guaranteed to reside, and Λ is used as a hard momentum cutoff in the effective field theory. Among all d-dimensional operators, we define Λ so that the largest dimensionless coupling λ is equal to unity. Unless otherwise noted, we will assume that all other λ are of order one.

In the first two columns of Table I, we exhaustively enumerate all possible lepton number violating operators of mass dimension less than or equal to 11. All together, this amounts to 129 different types of operators, most of which, 101 to be exact, are of dimension 11 and consist of six fermion and two Higgs fields. Remaining are 21, 6, and 1 operators of dimension nine, seven, and five, respectively. The dimension-nine operators can be of two different kinds, as defined by their respective field content. They either contain four fermion and three Higgs fields or simply six fermion fields with no Higgs field content. For consistency, we use the notation of Ref. [2], where such a listing was first introduced. Our operator naming scheme is also derived from the same list, which we trivially extend to include 21 elements only mentioned in that analysis. These are the dimension-nine and dimension-11 LNV operators that can be constructed from the ''product'' of the previously listed dimension-five and dimension-seven operators with the SM Yukawa interactions. We individually identify those operators with the same field content but different $SU(2)_L$ gauge structure with an additional roman character subscript added onto the original designation from [2]. This is done in order to render our discussion of the various operators clearer, since specific gauge structures can play an important role in the derived energy scale and predictions of a given operator. Note that we neglect effective operators that contain SM gauge fields, since, as argued in [2], these are not typically generated by renormalizable models of new physics.

Our notation is as follows.

$$L = \begin{pmatrix} \nu_L \\ e_L \end{pmatrix} \quad \text{and} \quad Q = \begin{pmatrix} u_L \\ d_L \end{pmatrix} \tag{2.2}$$

are the left-handed lepton and quark $SU(2)_L$ doublets, respectively. e^c, u^c, and d^c are the charge conjugate of the $SU(2)_L$ singlet right-handed charged-lepton and quark fermion operators, respectively. Conjugate fields are denoted with the usual ''bar'' notation ($\bar{L}$, $\bar{Q}$, $\bar{e}^c$). For simplicity, we are omitting flavor indices, but it is understood

that each matter fermion field comes in three flavors. All matter fields defined above are to be understood as flavor eigenstates: all SM gauge interactions, including those of the W boson, are diagonal. Without loss of generality, we will also define the L and e^c fields so that the charged-lepton Yukawa interactions are flavor diagonal.

We take the $SU(2)_L$ doublet Higgs scalar to be

$$H = \begin{pmatrix} H^+ \\ H^0 \end{pmatrix}, \tag{2.3}$$

and assume that, after electroweak symmetry breaking, its neutral component acquires a vev of magnitude $v \approx 0.174$ TeV,[4] thus spontaneously breaking the electroweak gauge symmetry $SU(2)_L \times U(1)_Y \to U(1)_{\rm em}$. In Table I, the components of the $SU(2)_L$ doublets are explicitly listed and labeled with $i, j, k, \ldots = 1, 2$. In order to form gauge singlets, operators are contracted either by the antisymmetric tensor ϵ_{ij}, defined such that $\epsilon_{12} = 1$, or by trivial contractions with a conjugate doublet field. Different gauge contractions are partially responsible for the wide variety of operator structures encountered in this study.

In order to avoid unnecessarily messy expressions, several features are missing from the operators as listed in Table I. To begin, $SU(3)_c$ color indices are suppressed in these expressions. Color contractions are only implied here because $SU(3)_c$ is an unbroken symmetry of the SM and hence there is no sense in distinguishing the various quark field components. We assume that the parent ultraviolet completion to each operator treats the color gauge symmetry properly by introducing appropriately chosen heavy colored particles to render the theory gauge invariant. Slightly more serious is the omission of flavor indices to label the fermion generations. For most of this analysis, we assume that all new physics effects are generation universal and, thus, flavor independent. This is not guaranteed to be the case, as is painfully obvious within the SM. One will also note that, depending on the $SU(2)$ structure of the effective operator, different flavor-dependent coefficients will be strictly related. For example, including flavor-dependent couplings $\lambda^1_{\alpha\beta}$, $\mathcal{O}_1$ should read $\lambda^1_{\alpha\beta} L^i_\alpha L^j_\beta H^k H^l \epsilon_{ik} \epsilon_{jl}$, where $\lambda^1_{\alpha\beta} = \lambda^1_{\beta\alpha}$ (symmetric) for all $\alpha, \beta = e, \mu, \tau$. On the other hand, $\mathcal{O}_{3a}$ should read (for fixed Q and d^c flavors) $\lambda^{3_a}_{\alpha\beta} L^i_\alpha L^j_\beta Q^k d^c H^l \epsilon_{ij} \epsilon_{kl}$, where $\lambda^{3_a}_{\alpha\beta} = -\lambda^{3_a}_{\beta\alpha}$ (antisymmetric) for all $\alpha, \beta = e, \mu, \tau$. Large differences among the various flavor structures of each operator may very well exist. Flavor is an important facet of LNV phenomenology, and is addressed where relevant within the text.

[4]Our numerical value for v is distinct from many treatments of the SM where v is taken to be 0.246 TeV. These are equivalent up to a factor of $\sqrt{2}$ and are both valid provided a consistent treatment of the interaction Lagrangian.

The final feature missing from our notation is explicit Lorentz structure. Each operator must, of course, form a Lorentz scalar, but there are numerous field configurations that can bring this about. The Higgs field is a scalar, and as such, transforms trivially under the Lorentz group and is thus of no relevance to this discussion. The fermions, however, transform nontrivially and their contractions must be accounted for in each operator. Simple combinatorics dictate that there are at most 45 such possibilities for the six-fermion operators that comprise the bulk of our sample, 3 in the four-fermion case, and only 1 for the lone dimension-five operator. Additionally, each contraction can be made in a variety of ways, corresponding to the bilinear Dirac operators $\mathbf{1}$, γ^μ, and $\sigma^{\mu\nu} = \frac{i}{2}[\gamma^\mu, \gamma^\nu]$ of the scalar, vector, and tensor types, respectively. Since we are dealing with chiral fields, the addition of the γ_5 matrix to form the pseudoscalar and axial-vector bilinears is redundant. While this helps reduce the number of possibilities, the task of listing, categorizing, and analyzing all possible Lorentz structures for each operator is still quite overwhelming and is not undertaken in this general survey. Fortunately, different Lorentz structures for the same operator-type lead to the same predictions up to order one effects. This is especially true for the interesting operators characterized by TeV Λ scales. We shall quantify this statement and mention specific structures when relevant. That being said, the Lorentz structure of an effective operator can suggest a lot of information about its parent renormalizable model. For example, it can suggest the spin of the heavy intermediate states and the forms of various vertices.

Armed with these operators, we can calculate the amplitude of any $\Delta L = 2$ LNV process. It is important to emphasize that, when addressing the phenomenological consequences of any particular operator $\mathcal{O}$, we assume that it characterizes the dominant tree-level effect of the new heavy physics, and that all other effects—also characterized by other LNV effective operators of lower mass dimension—occur at higher orders in perturbation theory. Our approach is purely diagrammatic, in that we begin with an operator-defined vertex and then proceed to close loops and add SM interactions as needed to yield the correct external state particles. In this sense, special care must be taken to respect the chiral structure as defined by each operator. In order to reach the intended external states, to couple to particular gauge bosons, or to close fermion loops, one must often induce a helicity flip with a SM mass insertion. We express these inserted fermion masses in terms of the respective Yukawa couplings, y_f ($f = \ell, u, d$), and the Higgs vev, v. The Higgs field can be incorporated into this procedure in a number of ways. We treat the two charged and single neutral Nambu-Goldstone Higgs bosons, $H^\pm$ and H^0, respectively, within the Feynman-'t Hooft gauge as propagating degrees of freedom with electroweak scale masses. The physical neutral Higgs, h_0, can

be either chosen to propagate as a virtual intermediate state, or couple to the vacuum with amplitude v.

In order to avoid the task of explicitly evaluating a huge number of multiloop Feynman diagrams, we succumb to approximate LNV amplitudes based on reasonable assumptions and well-motivated rules. Our methodology is motivated by exact computations with one-loop, dimension-seven operators where the work is analytically tractable, as well as on general theoretical grounds. For select operators, we have also checked our assumptions against predictions from ultraviolet complete models with success. In order to perform a particular calculation, we draw the appropriate diagram(s), taking care that no momentum loop integral vanishes by symmetry reasons. This step is potentially quite involved, as multiple diagrams can give sizable amplitude contributions depending on the characteristic energy transfer in the system, not to mention the cumbersome Dirac algebra within the respective loops. Given the high, often super-TeV, mass scale associated with our calculations, it is often convenient to work in the gauge field basis where each boson state is associated with a single SM group generator, as is natural before electroweak symmetry breaking. In a similar sense, all fermions, including those of the third generation, are taken to be massless to zeroth order. All masses are included perturbatively where needed via mass insertions. At first guess, it would seem that our results are only valid in the rather subjective limit $\Lambda \gg v$. By direct comparison with other more complete approximations, however, we find that our predictions are very reasonable at all scales above 0.5 TeV. Keeping all of this in mind, we apply the following ''rules'' to obtain approximate amplitude expressions.

(1) *Trivial numerical factors.*—A number of numerical factors can be read off trivially from the Feynman diagrams. Specifically, one can extract the presence of the suppression scale $\Lambda^{-(d-4)}$ directly from the dimension d operator, as well as the dimensionless coupling constants λ. Generally, λ is a generation-dependent quantity, but for lack of any experimental evidence to the contrary, we take $\lambda = 1$ universally unless stated otherwise. In the case of scenarios already constrained by current data, we will relax this assumption to ''save'' the operator and comment on the phenomenological consequences of the change.

Furthermore, various factors of the electroweak scale v may be extracted from the operator's Higgs field content, in addition to fermion/gauge boson mass terms. In this way, we may also include the various Yukawa and gauge coupling factors y_f ($f = \ell, u, d$) and g_i, respectively, where i runs over the three SM gauge groups. For simplicity, we neglect the gauge subscript i in further analytic expressions. Finally, a color factor of 3 associated with each quark loop should also be included in our computations, but can (and will) be neglected for simplicity from algebraic expressions where order one factors are irrelevant and only serve to render expressions more cumbersome. We note that all coupling constants are subject to renormalization group running. In particular, those occurring within a loop should be evaluated at the scale Λ. We neglect this order one effect since it is most important at large Λ scales where operators tend to have less of a phenomenological impact due to the $(1/\Lambda)^n$ suppression.

(2) *Loop factors.*—In all of our calculations, we assume that each operator defines an effective field theory, characterized by the scale Λ. This implies that all momentum integrals are effectively cut off at Λ, above which new states will emerge to regularize the theory. Divergences in such loops tend to cancel the large scale suppressions inherent to the bare operators, and thus enhance predicted LNV rates. Specific divergences can be determined by simple power counting of momentum factors. Of course, multiple loop integrals are often convoluted to the point where substantial simplification is needed to determine the dominant divergent term. Such a complication is in part due to the numerator of the Dirac propagators, which include single momentum factors and must therefore be present in pairs to contribute effectively to an ultraviolet divergence. The process of adding loops to induce Λ power-law divergences should only be pursued to the point where the suppression of the induced effective term is no less than Λ^{-1}. Any further divergent contribution must be treated as a renormalization to lower order terms, and hence, can only add small finite corrections to the total amplitude. In any case, those diagrams with the smallest scale suppressions are not always the most dominant, as will become clear later when we discuss specific results.

In addition to power-law divergences, each loop is also associated with a numerical suppression factor. This arises from the proper normalization of the loop four-momentum integral as a factor of $(2\pi)^{-4}$, the characteristic phase space ''volume'' of a quantum state. It allows one to view the integral as a coherent sum over all possible intermediate configurations in a consistent way. Partially evaluating these integrals for a number of examples, one quickly finds that two powers of π cancel with the four dimensional Euclidian space solid angle $\int d\Omega_4$. We introduce a suppression factor of $(16\pi^2)^{-1} \sim 0.0063$ for each diagram loop, which tends to offset enhancements from associated divergent factors. A quadratically divergent loop diagram is often proportional to the lowest order contribution times $(1/16\pi^2)(\Lambda/v)^2$ to the power n (number of

loops in the diagram). This contribution is larger than the leading order one if $\Lambda > 4\pi v \sim 2$ TeV for any number of loops. The situation is often more involved, as many loops turn out to be logarithmically divergent or even convergent. The important conclusion is that adding loops is not an efficient way to enhance LNV rates at the low scales accessible to future experiments. This fact is demonstrated by example in Sec. III.

Finally, as already alluded to, many diagram loops will exhibit logarithmic divergences, as is the standard case in renormalizable theories involving fermion and vector fields. This occurrence typically reflects the differences between the two characteristic scales inherent to the system, namely Λ and v, and are of the general form $\xi \log^n(\Lambda/v)$ for some power n. ξ is a small, loop suppressed, dimensionless coupling coefficient. Numerically, these logarithms are much softer than their quadratically divergent counterparts seen elsewhere in the diagrams and can safely be neglected.

(3) *Intermediate states.*—We treat all virtual intermediate states, outside of loops, as if they carry the characteristic momentum of the interaction Q and neglect Dirac structure, unless stated otherwise. In particular, Goldstone bosons are assigned the propagator $(Q^2 - M_g^2)^{-1}$ and fermions are assigned $(Q - M_f)^{-1}$. In the case of an intermediate neutrino, this reduces to a simple factor of Q^{-1} for all realistic Q values. Hence, for very low-energy processes ($Q \ll 100$ MeV), neutrino exchange diagrams tend to dominate LNV rates.

(4) *Lorentz structure.*—For the purposes of our analysis, we assume that all Lorentz contractions between fermions are scalarlike. As previously mentioned, the absolute magnitude of most LNV amplitudes is robust under this assumption up to order one factors. The only qualitative exception to this occurs in some cases involving fermion bilinear terms with a tensor Lorentz structure $(\bar{\psi}'\sigma_{\mu\nu}\psi)$. This factor, when coupled between two fermions contracted in a loop, will yield a vanishing rate due to its antisymmetry inside of a trace, since $\mathrm{Tr}(\sigma_{\mu\nu}) = 0$. This can be bypassed by introducing a new momentum vector into the trace, implying the addition of another loop. In most cases, this is most efficiently accomplished with a new gauge boson line, which is accompanied by a logarithmic divergence. The combination of both factors leads to a marginal amplitude suppression (with respect to the same operator where all fermion bilinears are Lorentz scalars) for all energies of interest.

With these approximations in hand, it is a simple matter to estimate the amplitude associated with any given diagram. Still, one must wonder about the uncertainty induced onto the calculations by such varied assumptions. Can results obtained by such methods supply valid physical predictions? The answer, of course, depends on the question that is being asked. Here, we will only be interested in estimating order of magnitude effects, including what value of Λ is required in order to explain the observed neutrino masses and, once Λ is so constrained, what is the order of magnitude of other related observable effects.

One may wonder whether a more detailed estimate of the effects of each individual operator would lead to more reliable results. The answer is negative. It is easy to show that different renormalizable theories that lead to the same effective operator at tree level will mediate different processes at the loop level with different relative strengths. Furthermore, the derived cutoff scales inherit the uncertainty from the absolute value of the heaviest neutrino mass, which is only loosely bounded between 0.05 eV and 1 eV by the extracted atmospheric mass-squared difference [3] and tritium beta-decay kinematic measurements [4,5]. This is an order of magnitude uncertainty that cannot be avoided even if one were to perform a detailed computation within a well-defined ultraviolet complete theory.

In summary, given all approximations and uncertainties, our results are only valid up to $\pm$ an order of magnitude. In this spirit, one need not explicitly consider order one factors that will necessarily yield negligible corrections by these standards. Such a large error tolerance supplies the need for care when interpreting results. In particular, one should not place too much emphasis on any one bound or prediction, unless it is very robust, i.e., able to withstand variations of at least a factor of 10. Of course, for those operators constrained by several different independent sources one can, and should, take more marginal results seriously.

Neutrino masses and the scale of new physics

Having defined the set of LNV operators, we now extract the scale of new physics from the direct comparison of radiatively generated neutrino-mass expressions to their observed values. Since there are three light neutrino masses, we will use the heaviest of these to set the overall mass scale. Neutrino oscillation data, currently providing the only evidence for neutrino masses, constrain the relative magnitudes of the mass eigenstates but not the overall scale [1]. Such data only supply a lower bound on the heaviest neutrino mass, derived from the largest observed mass-squared difference $\Delta m_{13}^2 = |m_3^2 - m_1^2| \approx 0.0025\ \mathrm{eV}^2$, the atmospheric mass-squared difference [3]. At least one neutrino mass must be greater than $\sqrt{\Delta m_{13}^2} \approx 0.05$ eV. Neutrino oscillations also teach us that the next-to-heaviest neutrino weighs at least $\sqrt{\Delta m_{12}^2} \approx 0.009$ eV (the solar mass-squared difference), in such a way that the ratio of the heaviest to the next-to-heaviest neutrino

masses is guaranteed to be larger than, approximately, 0.2. No lower bounds can be placed on the lightest neutrino mass. An upper bound on the heaviest neutrino mass is provided by several nonoscillation neutrino probes. Cosmology provides interesting constraints on the sum of light neutrino masses, but these are quite dependent on unconfirmed details of the thermal history of the universe and its composition [6]. Most direct are kinematic measurements of the tritium beta-decay electron endpoint spectrum [7]. Both types of probes provide upper bounds near 1 eV, likely to improve in coming years. We choose to perform our calculations assuming the mass scale $m_\nu \approx 0.05$ eV, corresponding to the experimental lower bound. In this way, each extracted operator scale Λ, inversely related to the neutrino mass, represents a loose upper bound. Since most rates for LNV observables are proportional to some inverse power of Λ, this choice implies the added interpretation that, all else remaining equal, our results for such rates should conservatively reflect lower limit predictions.

LNV neutrino masses are nothing more than self-energy diagrams evaluated at vanishing momentum transfer. These must couple together the left-handed neutrino state ν_α with the right-handed antineutrino state ν_β, as shown schematically in diagram (a) of Fig. 1. Here the flavor indices α and β can accommodate any of the three lepton flavors ($\alpha, \beta = e, \mu, \tau$). The derived Majorana masses $m_{\alpha\beta} = m_{\beta\alpha}$ are generally complex. The large gray circle in this diagram represents all possible contributions to the neutrino mass. Specifically, it contains the underlying $\Delta L = 2$ operator along with all modifications needed to yield the correct external state structure. This includes such objects as loops, additional gauge boson propagators, and SM coupling constants. Generally, several diagrams can contribute to this mass generation, but special care must be taken that these are not proportional to any positive power of Q, the momentum carried by the neutrino legs, as this would not lead to a nonzero rest mass correction.

Diagrams (b)–(e) of Fig. 1 are examples that serve to illustrate some typical features encountered in our effective operator-induced self-energy calculations. The underlying LNV operators shown in each diagram contain six fermion fields and are therefore of dimension nine or 11, as are the majority of the analyzed operators. Each of these diagrams generates an effective dimension-five interaction

$$\mathcal{L}_5 = \xi^{(5)}_{\alpha\beta} \frac{(L^\alpha H)(L^\beta H)}{\Lambda}, \tag{2.4}$$

where $\xi^{(5)}_{\alpha\beta} = \xi^{(5)}_{\beta\alpha}$ is a generation-dependent coupling constant that is calculable, given the structure of the original operator. This is easily verifiable via direct power counting, despite differences in dimension, loop number, field content, and helicity structure. It turns out that most operators, especially those characterized by super-TeV scales, possess this property.

We describe each sample diagram in turn to point out important features. A subset of the subtleties described below is encountered when estimating the neutrino masses $m_{\alpha\beta}$ for the entire effective operator set. Diagram (b) is a simple two-loop radiatively generated mass term proceeding from dimension-nine operators, such as $\mathcal{O}_{11_b} = L^i L^j Q^k d^c Q^l d^c \epsilon_{ik} \epsilon_{jl}$, containing the fermion structure $f_L f^c_R f'_L f'^c_R$, where the fields f and f' are contracted into loops with mass insertions that supply the needed field chirality flip. Masses arising from such operators are proportional to two powers of fermion Yukawa couplings. Strictly speaking, allowed fermions from all three generations traverse the closed loops and contribute to the mass. However, assuming universal new physics coupling constants, third generation fermions will strongly dominate the induced neutrino mass. In cases such as these, one can freely suppress couplings to the lighter two generations without modifying the expected value of Λ. Since dia-

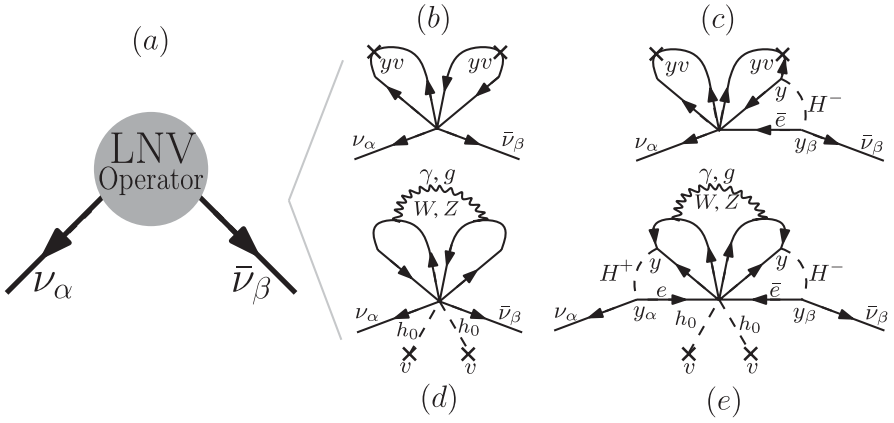

FIG. 1. Sample diagrams that radiatively generate Majorana neutrino masses. Diagram (a) is representative of all operators that can generate the needed external state neutrinos. This usually proceeds via loop contractions and other couplings, hidden within the light gray region. Diagrams (b)–(e) help illustrate the methodology of this analysis. Despite obvious differences, all of these generate effective dimension-five interactions of calculable strength. See the text for more details.

grams arising from the majority of our operator set contain at least one loop of this kind, this property proves quite useful when attempting to avoid low-energy nuclear physics constraints, as will be discussed in more detail later.

Diagram (d) involves an operator of dimension 11, such as $\mathcal{O}_{22} = L^i L^j L^k e^c \bar{L}_k \bar{e}^c H^l H^m \epsilon_{il} \epsilon_{jm}$, but has a similar structure to diagram (b) since both neutral Higgs fields h_0 couple to the vacuum, yielding a v^2 factor. In this case, the parent underlying operators contain the fermion structure $f_{L(R)} f^c_{L(R)} f'_{L(R)} f'^c_{L(R)}$, or simple variants thereof. From this, it is clear that such operators will create and annihilate the *same* field, and one can close the fermion loops without mass insertions. A little thought reveals that such loops, if left on their own, will vanish by symmetry, since $\int d^4k [k^\mu / g(k^2)] = 0$ for all functions $g(k^2)$. Hence, nonzero neutrino masses only appear at a higher order in perturbation theory (i.e., we need to add another loop). To maintain the chiral structure of the diagram, a gauge boson line insertion is always the most effective. The specific gauge field required in this step depends critically on the quantum numbers of the fermions f and f' contained in the operator itself and must be determined on a case-by-case basis. The absence of Yukawa dependence renders the estimated value of the cutoff scale Λ insensitive to the values of the dimensionless operator couplings (λ), given the way Λ is defined. Notice that this three-loop diagram, like diagram (b), predicts an anarchic neutrino Majorana mass matrix, currently allowed by the neutrino oscillation data [8]. That is, up to order one corrections, all entries are of the same magnitude, $m_\nu \approx 0.05$ eV. This is in contrast to the remaining sample diagrams (c) and (e), which both suggest flavor-structured mass matrices.

Dimension-nine operators, such as $\mathcal{O}_{19} = L^i Q^j d^c d^c \bar{e}^c \bar{u}^c \epsilon_{ij}$, yielding diagram (c) have the peculiar property that, upon expanding out the various $SU(2)_L$ contractions in terms of component fields, no $\nu_\alpha \nu_\beta$ content is present to form the external legs of a mass diagram. Here the LNV is introduced via the fermion structure $\nu_\alpha e_{R\beta}$, which annihilates a left-handed neutrino and creates a left-handed positron. Hence, to tie in the needed antineutrino line, one must both flip the charge lepton helicity and carry away the excess charge with some bosonic state. Of course, such a charged boson is guaranteed by charge conservation to be needed elsewhere in the system to close some f/f' loop. In this particular example, the process is illustrated by the exchange of a charged Higgs Goldstone boson H^-. The crucial point is that this mass is necessarily proportional to a charged-lepton Yukawa coupling y_{ℓ_β}, of the *same* flavor as the external neutrino, since we are working in the weak eigenbasis where the gauge couplings and the charged-lepton Yukawa couplings are flavor diagonal. By symmetry, the contribution to the $m_{\alpha\beta}$ entry of the neutrino-mass matrix is proportional to $y_{\ell_\alpha} + y_{\ell_\beta}$, which reduces to the largest coupling y_{ℓ_β} in the realistic case of hierarchial charged-lepton Yukawa couplings.

Finally, diagram (e) yields a five-loop suppressed neutrino self-energy originating from a dimension-11 LNV operator such as $\mathcal{O}_{36} = \bar{e}^c \bar{e}^c Q^i d^c Q^j d^c H^k H^l \epsilon_{ik} \epsilon_{jl}$. This represents the most complicated structure considered in this analysis. As in diagram (c), no explicit $\nu_\alpha \nu_\beta$ structure is available in the underlying operator, but in this case all of the LNV arises from $e^c_{R\alpha} e^c_{R\beta}$-type interactions. Curiously, this interaction already flips helicity as it annihilates a left-handed positron and creates a right-handed electron. Unfortunately, being an $SU(2)_L$ singlet, e_R only couples to the neutrino via a charged Higgs induced Yukawa interaction; therefore, this amplitude must be proportional to the product $y_{\ell_\alpha} y_{\ell_\beta}$ to yield a legitimate neutrino-mass contribution. One might imagine that the Higgs fields contained in the LNV operator could be used to produce the needed neutrino legs, but this is not possible since the resulting loop would have a structure of the form $\int d^4k \frac{k^\mu + Q^\mu}{g(k^2)} \propto Q^\mu$ which vanishes in the "rest mass" limit. It is clear that both Higgs fields must again couple to the vacuum and the needed flip must come from the other fermion loops. The resulting loop integrals can be separated into two convoluted pieces corresponding to both loop/leg pairs. A little thought reveals that each loop set contains three fermion lines whose associated integral is again proportional to the momentum of the external neutrino, and thus is not a valid mass correction. To fix this last problem without further complicating the chiral structure, one can add a gauge boson exchange between the fermion loops, as was also done in diagram (d).

Despite the dominance of the generated dimension-five interactions described by Eq. (2.4) for the majority of the studied LNV operators, we find that this need not be the case for all of them. For some operators, the dimension-five neutrino-mass effective operator, Eq. (2.4), occurs at higher order in perturbation theory than the dimension-seven neutrino-mass effective operator [schematically, $(LH)^2 H^2$]. For these, the neutrino-mass matrix is generated after electroweak symmetry breaking from

$$\mathcal{L}_{57} = \frac{\xi^{(5)}_{\alpha\beta}}{16\pi^2} \frac{(LH)(LH)}{\Lambda} + \xi^{(7)}_{\alpha\beta} \frac{(LH)(LH)H\bar{H}}{\Lambda^3}, \quad (2.5)$$

where $\xi^{(7)}_{\alpha\beta}$ are new calculable coefficients. This type of structure is present in the following operators:

$$\mathcal{O}_7,\ \mathcal{O}_{21_{a,b}},\ \mathcal{O}_{22},\ \mathcal{O}_{23},\ \mathcal{O}_{25},\ \mathcal{O}_{26_b},\ \mathcal{O}_{27_b},\ \mathcal{O}_{29_a},\ \mathcal{O}_{30_b},\ \mathcal{O}_{31},\ \mathcal{O}_{44_c},\ \mathcal{O}_{57}. \quad (2.6)$$

In general, they are associated with dimension-11 operators[5] whose mass diagrams are found trivially by connect-

[5]This also occurs with operator $\mathcal{O}_7$, which is of dimension nine. This operator is the exception, in that it explicitly contains three Higgs bosons, which naturally aids in building the needed v^4 factors in a way similar to that discussed in the text.

ing the external fermion loops and coupling the neutral Higgs fields to the vacuum. This adds two factors of the electroweak scale to the mass expressions. Dimensional analysis dictates that the fermion loops must conspire to yield an additional factor of v^2, usually from mass insertions utilized to flip helicities. For the dimension-seven operators in Eq. (2.5), the resulting neutrino-mass expression is proportional to v^4/Λ^3. If we assume, as is usually the case, that most of the dimensionless factors of Eq. (2.5) are common to both $\xi^{(5)}_{\alpha\beta}$ and $\xi^{(7)}_{\alpha\beta}$, we find $m_{\alpha\beta} \propto 1/16\pi^2 + v^2/\Lambda^2$. In such cases, the dimension-seven contribution is only relevant for operator cutoff scales $\Lambda \lesssim 4\pi v \approx 2$ TeV. Such low scales are seldom reached considering that these operators are efficient at mass generation at low orders and consequently do not possess the necessary suppression factors. Still, for completeness, we include these terms when relevant.

The third column of Table I, labeled $m_{\alpha\beta}$, presents our estimate for the operator-induced Majorana neutrino-mass expressions. These were derived based on the estimation procedure discussed earlier. Trivial order one factors, as well as the generation-dependent coupling constants λ, have been omitted, as already advertised. Flavor specific charged-lepton Yukawa couplings are explicitly denoted y_{ℓ_α} and y_{ℓ_β} to distinguish them from y_ℓ, y_u, and y_d, meant to represent α, β-independent Yukawa couplings. A summation over all "internal flavors" is assumed for each entry. For order one coupling constants, this sum is strongly dominated by third generation Yukawa couplings. Upon setting these mass expressions equal to the observed scale of light neutrino masses (0.05 eV), we extract the required cutoff scale Λ for each operator. This quantity, defined to be Λ_ν, is listed in column four in units of 1 TeV. Numerical results were obtained assuming the current best fit values for all SM parameters. Associated errors are negligibly small as far as our aspirations are concerned.

Figure 2 displays the distribution of extracted cutoff scales, Λ_ν. The histogram bars are color-coded to reflect the different operator mass dimensions. The distribution spans 13 orders of magnitude, from the electroweak scale to 10^{12} TeV. It is interesting to note the general trend of operator dimension with scale: as expected, higher dimension operators are characterized by lower ultraviolet scales. For operators associated with the lowest ultraviolet cutoffs, the lepton number breaking physics occurs at the same energy scale as electroweak symmetry breaking. In this case, one needs to revisit some of the assumptions that go into obtaining the bounds and predictions discussed here. Regardless, it is fair to say that some of these effective operators should be severely constrained by other experimental probes, as will be discussed in the next section.

The natural scale for most of the explored operators is well above 10 TeV, and thus outside the reach of future experimental efforts except, perhaps, those looking for neutrinoless double-beta decay. The remainder, however,

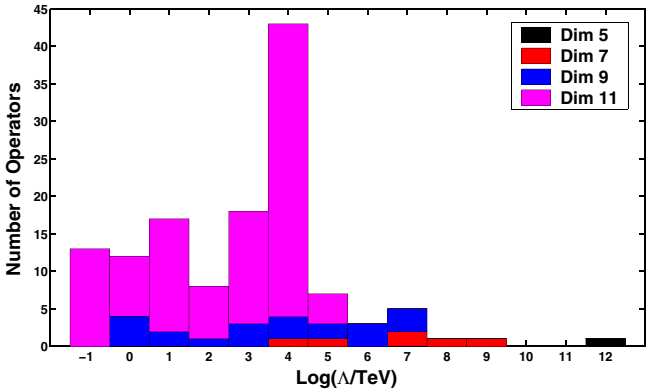

FIG. 2 (color online). A summary histogram of the scale of new physics Λ_ν extracted from the 129 LNV operators introduced in Table I. We assume a radiatively generated neutrino mass of 0.05 eV and universal order one coupling constants. The contributions of operators of different mass dimensions are associated with different colors (shades of gray), as indicated in the caption.

should yield observable consequences in next-generation experiments. This small subset arguably contains the most interesting cases on purely economic grounds, as they naturally predict tiny neutrino masses as well as TeV scale new physics, which is already thought to exist for independent reasons. It is aesthetically pleasing to imagine that all, or at least most, of nature's current puzzles can arise from the same source, as opposed to postulating various solutions at different energy scales. It is important to note that one can "push" more of the operators into the observable TeV window by modifying the coupling of the new physics to different fermion generations. In particular, since many of the induced neutrino masses depend upon fermion Yukawa couplings, one can efficiently reduce scales by simply and uniformly decoupling the third generation. In most cases this can yield a Λ_ν reduction of several orders of magnitude, a factor that can be further enhanced by also decoupling the second generation. Under these conditions, the resulting distribution, analogous to Fig. 2, would show the majority of the operators piled up near and slightly above the electroweak scale. A detailed exploration of this possibility would be impractical and is not pursued further. We would, however, like to emphasize that this strategy of decoupling the new physics from the *heavy* fermions is very nonstandard. In most cases, one is tempted to decouple *light* fermions from new physics, both because these lead to the strongest constraints and because one tends to believe that the large Yukawa couplings of third generation fermions are entangled with the physics of electroweak symmetry breaking.

Not all extracted cutoff scales are subject to a strong dependency on SM Yukawa couplings. In particular, the Λ_ν values for the majority of dimension-11 operators in the large histogram bar near 10^4 TeV would not shift down at

all under this hypothetical decoupling of the third generation from the new physics. These are the operators, as shown in diagram (d) of Fig. 1, whose induced neutrino-mass matrix is independent of the Yukawa sector. In such cases, $m_{\alpha\beta}$ are only functions of the various gauge couplings. As such, these constitute the most robust results of our analysis. These operators all predict an anarchic Majorana neutrino-mass matrix of overall scale given by $m_\nu = g^2/(16\pi^2)^3 v^2/\Lambda$, implying an energy scale $\Lambda_\nu \sim 10^5$ TeV. The only other "Yukawa invariant" cutoff scale estimate arises for the dimension-five operator $\mathcal{O}_1$. $\mathcal{O}_1$ captures the physics of all versions of the seesaw mechanism [9], and is at the heart of most of the model building currently done within the neutrino sector. Its ultraviolet completion can precede in only three distinct ways [10]. These possibilities are via the exchange of heavy gauge singlet fermions (type I seesaw), $SU(2)_L$ triplet scalars (type II seesaw) [11], $SU(2)_L$ triplet fermions (type III seesaw) [12], or some combination thereof. Its popularity is well founded for a number of reasons, including its underlying simplicity in structure as well as the purely empirical fact that it is the "lowest order means" of neutrino mass, and as such is easily generated by a "generic" LNV model. Additionally, the high scale associated with the seesaw mechanism can be easily incorporated within existing theoretical models and serves to help explain the observed baryon antisymmetry of the universe via leptogenesis [13].

For the purposes of direct observation, $\mathcal{O}_1$'s high cutoff scale, nearly 10^{12} TeV, places it well outside of the "detectable region" ($\Lambda \lesssim 10$ TeV) and renders it uninteresting for the purposes of our analysis. Of course, there always remains the possibility that $\mathcal{O}_1$ is generated by very weakly coupled new physics (or very finely tuned new physics [14]), in which case we expect to run into the new ultraviolet degrees of freedom at energies well below 10^{12} TeV. In the case of $\mathcal{O}_1$, it has been argued that new physics at almost any energy scale (from well below the sub-eV realm to well above the weak scale) will lead to light neutrino masses [15] without contradicting current experimental results. Such possibilities—related to the fact that the new physics is very weakly coupled—are not being explored here, as we always assume that the new degrees of freedom are heavier than typical experimentally accessible energy scales.

Armed with our derived new physics scales Λ_ν, we proceed to plug them back into the different irrelevant LNV operators and search for possible means of future observation as well as already existing constraints. Generally, those operators that yield the largest experimental signals have the lowest cutoff scales. We conclude that, if associated with neutrino masses, the effective cutoff scale Λ_ν of the following effective operators is constrained to be less than 1 TeV:

$$\mathcal{O}_{34},\ \mathcal{O}_{36},\ \mathcal{O}_{37},\ \mathcal{O}_{38},\ \mathcal{O}_{53},\ \mathcal{O}_{54_{a,b,c,d}},\ \mathcal{O}_{56},\ \mathcal{O}_{59},\ \mathcal{O}_{60},\ \mathcal{O}_{70}. \tag{2.7}$$

These may lead to observable effects at future high-energy accelerator facilities. Additionally, such low scales may also indirectly lead to observable effects in "low-energy" (but high sensitivity) experiments. There are more operators associated with slightly higher scales between 1 and 10 TeV that may manifest themselves experimentally via virtual effects. These are

$$\mathcal{O}_{16},\ \mathcal{O}_{17},\ \mathcal{O}_{18},\ \mathcal{O}_{19},\ \mathcal{O}_{35},\ \mathcal{O}_{43_{a,b,c}},\ \mathcal{O}_{50},\ \mathcal{O}_{52},\ \mathcal{O}_{55_{a,b,c}},\ \mathcal{O}_{57},\ \mathcal{O}_{58},\ \mathcal{O}_{65},\ \mathcal{O}_{68_{a,b}},\ \mathcal{O}_{73_a},\ \mathcal{O}_{75}. \tag{2.8}$$

These operators yield finite predictions for more than one observable, such that experimental efforts in seemingly unrelated fields can help constrain the class of possible LNV models or even help identify the true LNV model.

III. GENERAL OPERATOR CONSTRAINTS AND PREDICTIONS

There are, currently, bounds on LNV processes from a number of independent experimental sources [16,17]. Many of these are presently too mild to constrain the operators listed in Table I once their ultraviolet cutoffs Λ are set to the required value indicated by the presence of nonzero neutrino masses, Λ_ν. The situation, however, is expected to improve in the next several years with increased rare decay sensitivities and higher collider energies. Here we survey the experimental signatures of these operators in terms of the minimal scenarios described above. Specifically, we address the potential of neutrinoless double-beta decay (Sec. III A), rare meson decays (Sec. III B), and collider experiments (Sec. III C) to constrain the effective operators in question, assuming that, indeed, they are responsible for the observed nonzero neutrino masses. As before, we will use the approximations discussed in Sec. II, and warn readers that all the results presented are to be understood as order of magnitude estimates. The results, however, are useful as far as recognizing the most promising LNV probes and identifying different scenarios that may be probed by combinations of different LNV searches.

Most of this section will be devoted to probes of LNV via simple variants of the following process, which can be written schematically as

$$\ell_\alpha \ell_\beta \leftrightarrow d_\kappa d_\xi \bar{u}_\rho \bar{u}_\omega. \tag{3.1}$$

Greek subscripts run over all different fermion flavors. Given the assumed democratic models, coupled with our present lack of experimental information, one would expect that all flavor combinations are equivalent to zeroth order. Any indication to the contrary would signify important deviations from simple expectations, and thus begin to reveal the flavor structure of the new physics. The above

selected "golden modes" often yield the largest LNV rates, but this is not always the case. For example, some operators do not allow tree-level charged dilepton events, but rather prefer to include neutrino initial or final states. LNV processes with initial- and final-state neutrinos are extremely difficult to identify. The only hope of such discovery channels is, perhaps, via neutrino scattering experiments on either electron or nucleon targets, using well-understood neutrino beams. We point out that any neutrino/antineutrino cross contamination induces ambiguity onto the total lepton number of the incident beam and would serve as a crippling source of background for LNV searches. This reasoning rules out conventional superbeam [18] facilities as well as proposed neutrino factories [19], which contain both neutrino and antineutrino components, but does suggest modest possibilities for future beta beams [20]. Given projected beta-beam luminosities and energies along with the derived cutoff scales Λ_ν, it seems unlikely that LNV can be observed in such experiments. Another possible discovery mode involves only two external state quarks and an associated gauge boson as in the sample process $\ell_\alpha \ell_\beta \to d\bar{u} + W^-$. It turns out that the rates for such processes are generally suppressed for the majority of operators involving six fermion fields, as we are trading a phase space suppression for a stronger loop suppression. For those operators with only four fermion fields, the situation is not as straightforward and, in some cases, the three particle final state is preferred. Typically, the neutrino-mass induced cutoff scales of those operators are high ($\Lambda_\nu \gg 100$ TeV), so it would be quite difficult to observe such effects. Of course, any W-boson final state will either promptly decay leptonically, yielding missing energy and unknown total lepton number, or hadronically, reducing the reaction back to that of the golden mode.

Another possibility is to replace two or more of the external quark states in Eq. (3.1) with leptons in such a way as to preserve charge, baryon number, and $\Delta L = 2$ constraints. While many operators favor this structure, a little thought reveals that at least one external neutrino state is always present, which leaves only a missing energy signature, and little means of lepton number identification in a detector. Such events would not be clean, but of course, three final-state charged leptons and missing energy are enough to extract the existence of at least $\Delta L = 1$ LNV, provided that the number of invisible states is known to be no greater than 1. This last requirement is difficult to achieve in the presence of the large backgrounds and the limited statistics expected at future collider facilities, but should still be possible given a concrete model probed near resonance (see for example [21]). Therefore, while important and potentially observable, this mode is generally not the best place to look for LNV and is neglected in the remainder of our analysis. From this perspective, the only other relevant channel of LNV discovery is related to W and Z rare decays into final states with nonzero total lepton number. This possibility is briefly addressed in Sec. III B.

A. Neutrinoless double-beta decay

Here we probe the expectations for neutrinoless double-beta decay ($\beta\beta0\nu$) for each operator listed in Table I. $\beta\beta0\nu$ is the LNV ($\Delta L = 2$) process where, within a nucleus, two down quarks convert into two up quarks with the emission of two electrons but no neutrinos, or in the language of nuclear physics, $(A, Z) \to (A, Z+2) + e^- e^-$. See [22] and references therein for a comprehensive review. While precise computations of nuclear matrix elements are essential for making detailed predictions [23], the minimal parton-level description given above is adequate for the purposes of this study. There is a continuing legacy of cutting-edge experiments designed to search for $\beta\beta0\nu$ with no success to date.[6] Currently the ^{76}Ge half-life for this process is bounded to be greater than 1.9×10^{25} yr and 1.57×10^{25} yr at 90% confidence by the Heidelberg-Moscow [25] and IGEX [26] experiments, respectively. Future experiments are poised to improve these limits (for several different nuclei) by a couple of orders of magnitude within the next five to ten years [27].

If one assumes that $\beta\beta0\nu$ proceeds via the exchange of light Majorana neutrinos, its amplitude is proportional to the ee element of the Majorana neutrino-mass matrix,

$$m_{ee} = \sum_{i=1}^{3} m_i U_{ei}^2, \tag{3.2}$$

where m_i are the neutrino masses and U_{ei} are elements of the leptonic mixing matrix. With this, one can extract the upper bound $m_{ee} < 0.35$ eV (90% confidence level bound, [17]) from current experiments, while next-generation experiments are aiming at $m_{ee} \gtrsim 0.05$ eV[7] [27]. In general, LNV new physics will lead to additional contributions to $\beta\beta0\nu$, most of which are not proportional to m_{ee}. However, the amplitude for $\beta\beta0\nu$ can still be expressed in terms of an effective m_{ee}, m_{ee}^{eff}, which is an operator-specific quantity that will be used to analyze new models of LNV.

Here, we define six different "classes" of diagrams one can construct out of LNV irrelevant operators that contribute to $\beta\beta0\nu$ at the parton level. These are illustrated in Fig. 3, and classified by the dimension of the generated LNV interaction, depicted by large gray dots. In order to unambiguously separate the different classes, note that the gray circles are defined in such a way that all fermion and Higgs legs that come out of it are part of the "parent" operator $\mathcal{O}$ (and not attached via reducible SM vertices),

[6]There is currently a positive report of $\beta\beta0\nu$ at the 4.2σ level by a subset of the Heidelberg-Moscow Collaboration [24]. They report a measured half-life of $1.74^{+0.18}_{-0.16} \times 10^{21}$ yr which maps to $m_{ee}^{\text{eff}} \sim (0.2\text{–}0.6)$ eV. We choose to neglect this controversial result, which is still awaiting independent conformation.

[7]The parameter change from half-life to m_{ee} depends heavily on nuclear matrix element calculations. Current calculations induce an uncertainty of less than a factor of 4 on m_{ee} for most parent isotopes [23].

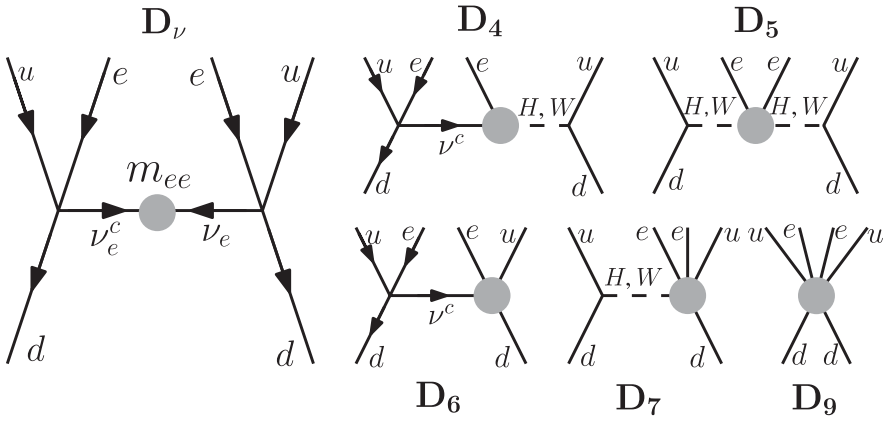

FIG. 3. The parton-level Feynman diagrams contributing to neutrinoless double-beta decay, labeled by the dimension of the underlying lepton number violating interaction, indicated by gray dots. Each diagram is generated, at some order in perturbation theory, by all analyzed interactions, but estimates of their magnitudes depend heavily on the details of the operators, including their associated scale Λ_ν, fermion content, and helicity structure.

while all other interactions are SM vertices. The dots should be viewed as hiding the underlying LNV interactions. In general, they contain a mixture of coupling constants and loop factors that must be evaluated explicitly for each diagram. It is important to emphasize that the contribution of a generic operator $\mathcal{O}$ to $\beta\beta0\nu$ will consist of contributions from all different classes, while usually dominated by one of them. We show the lepton number conserving electroweak vertices (pointlike) as effective four-fermion interactions, justified by the low-energy scale of nuclear beta decays. The dotted lines indicate the exchange of W bosons, labeled by W and H (charged Higgs Goldstone boson). Helicity arrows are explicitly included where uniquely determined, implying that the arrowless legs can have any helicity.

D_ν describes the standard scenario of $\beta\beta0\nu$ mediated by light Majorana neutrinos. It is simply two electroweak vertices held together by a Majorana mass term on which two neutrinos are annihilated. The amplitude for this diagram is proportional to m_{ee}, as defined in Eq. (3.2). The dependence on such a neutrino mass is intuitively clear considering the need for a helicity flip on the internal neutrino line. The remaining diagrams are qualitatively different from this standard case. Most importantly, none of them require "helicity flips" and are therefore not directly proportional to neutrino masses. They are, however, proportional to inverse powers of the new mass scale Λ_ν, and hence also suppressed. These effects are not entirely independent, since the value of Λ_ν was extracted from the requirement that neutrino masses are small, but correlations are relaxed enough to allow nontrivial consequences. It is this partial decoupling from neutrino masses that allows larger than naively expected contributions to $\beta\beta0\nu$ from some of the LNV irrelevant operators. Before proceeding, we make the trivial observation that the amplitudes following from D_ν, D_4, and D_5 are additionally proportional to two powers of Cabibbo-Kobayashi-Maskawa (CKM) matrix elements, namely $|V_{ud}|^2$, whereas D_6 and D_7 are only proportional to one power of V_{ud}.[8] The tree-level diagram D_9 has no CKM "suppression." While this is a purely academic fact in the case of $\beta\beta0\nu$ ($|V_{ud}| \sim 1$), it leads to important consequences for analogous rare decays that depend on the much smaller off-diagonal CKM matrix elements. We will return to these in the next subsection.

For a given operator, the relative size of each diagram's contribution to the total decay rate depends on many factors including the operator's dimension, scale, fermion content, and helicity structure. The dominant contributions must be calculated on a case-by-case basis. Generally, the high scale operators ($\Lambda_\nu \gtrsim 10$ TeV) are dominated by the two dimension-four diagrams D_ν and D_4 since many factors of Λ_ν will be canceled by divergent loops inside the gray dots, thereby minimizing the $1/\Lambda_\nu$ suppression. All else being equal, D_ν is the strongest of the pair since it is enhanced by $\sim Q^{-2}$ from the two propagating neutrino lines as opposed to only $\sim Q^{-1}$ for the one neutrino case shown in diagram D_4. For those operators with no tree-level $\nu\nu$ field content, D_4 can still be very important, but its dominance is nevertheless rare. As discussed in Sec. II, these are precisely the operators that have the greatest loop suppressions and consequently lower energy scales suggesting the need for diagrams beyond D_4. The effects of low cutoff scale operators ($\Lambda_\nu \lesssim 1$ TeV) are not severely suppressed by $1/\Lambda_\nu$ (by definition), so the dominant diagrams will typically be of the highest dimension allowed by the tree-level structure of the operator. For such low

[8]This is true provided that we assume no flavor structure for the underlying operator, or, equivalently, that all dimensionless coupling constants are order one. If one is motivated by experiment to postulate a minimally flavor-violating scenario, to perhaps ease constraints from flavor changing neutral currents, the statement must be modified accordingly.

scales and for operators of the following schematic form, $dd\bar{u}\,\bar{u}\,\bar{e}\,\bar{e}$ (dimension nine) or $dd\bar{u}\,\bar{u}\,\bar{e}\,\bar{e}\,H_0H_0$ (dimension 11), D_9 always dominates the $\beta\beta0\nu$ rate yielding amplitudes proportional to $1/\Lambda_\nu^5$ and v^2/Λ_ν^7, respectively. For intermediate scales, and when the operator's field content does not directly support $\beta\beta0\nu$ due to lack of quark fields, the situation is not as straightforward and one must perform the relevant computations to determine the dominant diagrams. Still, it should be noted that diagrams containing internally propagating neutrinos are enhanced by inverse powers of Q and maintain a slight advantage over their neutrinoless counterparts. One can thus generally expect diagram D_6 to dominate the decay rates for low Λ_ν scale operators when D_9 is suppressed. The opposite is true for interactions taking place at higher energies in, for example, next-generation colliders, as discussed in Sec. III C.

Since each diagram in Fig. 3 can have different external helicity structures, the different contributions to the total rate will be added incoherently, thus eliminating the effects of interference. There are some case-specific coherent contributions that we neglected in our treatment since most rates are dominated by a single diagram. Another potential difference among the different contributions is related to nuclear matrix element calculations: can the calculations done assuming $\beta\beta0\nu$ via the standard light Majorana neutrino exchange scenario of diagram D_ν be applied to the more general cases encountered here? We have nothing to add to this discussion except to naively note that there is no obvious reason why such rates should be severely suppressed or enhanced relative to the standard scenario. We therefore assume that all nuclear matrix elements are identical and can be factored out of the incoherent sum. We assume that this approximation is not more uncertain than the other sources of uncertainty inherent to our study (likely a very safe assumption).

As drawn, each diagram D_i contributes to the amplitude that characterizes $\beta\beta0\nu$. For example, the amplitude associated with D_ν is proportional to

$$\mathcal{A}_{D_\nu} \equiv m_{ee}\frac{|V_{ud}|^2G_F^2}{Q^2}, \tag{3.3}$$

where G_F is the Fermi constant. The remaining diagrams will contribute with $\mathcal{A}_{D_i} \propto \zeta(v,Q)\Lambda^{4-i}$, up to a dimensionless coefficient containing various numerical/loop factors, as well as general scale dependencies parametrized by some power of the ratio v/Λ. The function $\zeta(v,Q)$ has mass dimension $i-9$ so that all $\mathcal{A}_{D_i}$ have the same mass dimension. Note that all aspects of $\mathcal{A}_{D_i}$ are calculable given a LNV operator and diagram. We can analyze each operator in terms of an effective $m_{ee}^{\rm eff}$, defined in terms of the underlying dimension-nine amplitude $\mathcal{A}_{D_i}$ by

$$m_{ee}^{\rm eff} = \frac{Q^2}{G_F^2|V_{ud}|^2}\sqrt{\sum_i \mathcal{A}_{D_i}^2}, \tag{3.4}$$

where i runs over the set $\{\nu,4,5,6,7,9\}$ that labels the diagrams shown in Fig. 3, and $Q\sim 50$ MeV is the typical momentum transfer in $\beta\beta0\nu$. $m_{ee}^{\rm eff}$ can be directly compared with experiment and used to make predictions for future observations. A few comments are in order regarding this quantity. First, it is a useful derived object that has no direct connection to a real neutrino mass and is valid to arbitrarily large values. Note that in the case of Majorana neutrino exchange, $m_{ee}^{\rm eff} = m_{ee}$ only if $m_{ee} \ll Q$. When neutrino masses are greater than Q, $m_{ee}^{\rm eff} \propto 1/m$. Our definition of $m_{ee}^{\rm eff}$ also conforms to the use of large effective masses in [16]. The second comment is that, unlike the case of m_{ee}, which is valid for any process involving the exchange of electronlike Majorana neutrinos, $m_{ee}^{\rm eff}$ is case specific. It must be calculated separately for each process, as each one, in general, is composed of different diagrams. In particular, the calculations of the effective mass for $\beta\beta0\nu$ expressed here are not directly applicable to other LNV processes and should not be interpreted as such.

The $m_{ee}^{\rm eff}$ distribution extracted from all operators is shown in Fig. 4 assuming the scales Λ_ν derived in Sec. II and color-coded for convenience within the histogram. Specifically, we indicate in green (light gray) the operators that are characterized by sub-TeV scales and thus accessible to next-generation experiments via direct production. The blue (darkest gray) and red (dark gray) operators are characterized by scales between (1–5) TeV and (5–25) TeV, respectively, where virtual effects should be most important for collider searches. The majority of operators, shown in cyan (lightest gray), are suppressed by scales greater than 25 TeV and are hence quite difficult to observe in other search modes. We also explicitly label each operator within the histogram bars for easy identifi-

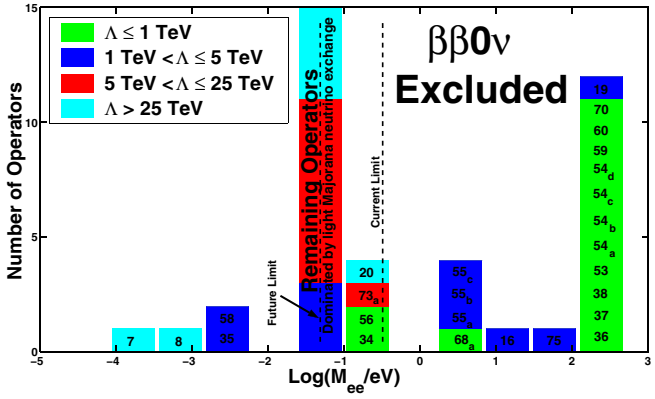

FIG. 4 (color online). $m_{ee}^{\rm eff}$ distribution derived for the neutrinoless double-beta-decay process as described in the text. The calculations were made assuming the scales Λ_ν derived in Sec. II, as well as universally order one coupling constants. The histogram bars are labeled explicitly with operator names and color-coded by their cutoff scales. Also shown in light gray is the region probed by next-generation experiments. The vertical axis is truncated at 15 operators to best display the relevant features of the plot.

cation and comparison. One should notice the expected general trend that increasing Λ_ν leads to a decrease in $m_{ee}^{\rm eff}$ and vice versa. The vertical axis is truncated at 15 operators, as the bar near 0.05 eV, dominated by the light Majorana neutrino exchange described above, would extend to nearly 100 operators. With broken vertical lines, we indicate the current 90% upper bound [17], $m_{ee}^{\rm eff} = 0.35$ eV, and the potential reach of future experiments.

This distribution, which spans over 6 orders of magnitude (from 10^{-4} eV to 10^2 eV), reveals many important features of the effective operator set. Beginning at the largest $m_{ee}^{\rm eff}$ values, we find that the 12 operators appearing near 300 eV all have the expected common feature of low-energy scales, including $\mathcal{O}_{19}$ with Λ_ν only just above the 1 TeV mark. Additionally, the contribution of the majority of these operators to $\beta\beta0\nu$ is dominated by the tree-level D_9 diagram. The exceptions are $\mathcal{O}_{54_{c,d}}$ and $\mathcal{O}_{70}$, all of which are characterized by sub 0.5 TeV scales and dominated by diagram D_6. Consequently, these are subject to a loop and Yukawa/gauge[9] suppression relative to their D_9 dominated cousins, but the difference is not visible given the resolution of the figure. It is interesting to note that these three operators have the correct quark and lepton content for large $\beta\beta0\nu$, but their $SU(2)_L$ gauge structures forbid large tree-level contributions. Similarly, operators $\mathcal{O}_{16}$, $\mathcal{O}_{55_{a,b,c}}$, $\mathcal{O}_{68_a}$, and $\mathcal{O}_{75}$ are also dominated by diagram D_6 accompanied by slightly higher cutoff scales. This drives down $m_{ee}^{\rm eff}$ significantly considering the leading one-loop scale suppressions of Λ^{-5} and Λ^{-3} for the dimension-11 and dimension-nine operators, respectively. We point out that operators $\mathcal{O}_{54_{a,b,c,d}}$ and $\mathcal{O}_{55_{a,b,c}}$ yield almost identical expressions for their respective $\beta\beta0\nu$ amplitudes (as well as their radiatively generated neutrino-mass expressions) with up and down quark Yukawa couplings exchanged. While this action enhances most of the $\mathcal{O}_{55}$ $\beta\beta0\nu$ couplings relative to those of $\mathcal{O}_{54}$, it also raises the $\mathcal{O}_{55}$ Λ_ν scale by nearly a factor of 4 and thus drives $m_{ee}^{\rm eff}$ down by orders of magnitude.

The remaining operators all predict $m_{ee}^{\rm eff} < 1$ eV, close to current experimental bounds. The histogram bar near 0.1 eV is composed of operators of very different Λ_ν scales. $\mathcal{O}_{34}$ and $\mathcal{O}_{56}$ are both characterized by low cutoff energy scales around 0.5 TeV, but, due to their fermion and helicity structure, their contributions to $\beta\beta0\nu$ are dominated by two-loop versions of diagram D_6. The neutrino-mass-required cutoff for $\mathcal{O}_{73_a}$ is around 7 TeV and its contribution to $\beta\beta0\nu$ is also dominated by diagram D_6. In this case, however, the two-loop version turns out to be larger than the allowed one-loop amplitude due to strong scale suppressions (the added loop reduces the cutoff dependency from Λ^{-5} to Λ^{-3}). This behavior is characteristic of operators with a larger value of Λ_ν. The $\Lambda_\nu = 40$ TeV operator $\mathcal{O}_{20}$ defines the lower edge of this histogram bar. It is dominated by the one-loop diagram D_6 enhanced by a top quark Yukawa coupling and, being a dimension-nine operator, is only suppressed by Λ^{-3} from the start. The next bar down contains operators dominated by D_ν. Most of these are suppressed by a very high-energy scale, but a small subset is characterized by scales $\Lambda_\nu <$ 25 TeV. In particular, operators $\mathcal{O}_{17}$, $\mathcal{O}_{18}$, and $\mathcal{O}_{57}$ are all cut off at 2 TeV but, due to their fermion content, they cannot participate in any of the nonstandard interactions of Fig. 3 at a low enough order in perturbation theory. Similarly, the intermediately scaled operators $\mathcal{O}_{43_{a,b,c}}$, $\mathcal{O}_{50}$, $\mathcal{O}_{52}$, $\mathcal{O}_{62}$, $\mathcal{O}_{65}$, and $\mathcal{O}_{69_b}$ have either the wrong fermion content or gauge structure to enhance any of the $\beta\beta0\nu$ diagrams (other than D_ν) to an observable level. These operators are important because their minimal forms are experimentally unconstrained yet still potentially observable to both next-generation $\beta\beta0\nu$ and collider experiments. The remaining histogram bars with $m_{ee}^{\rm eff} < 10^{-2}$ eV are not accessible to $\beta\beta0\nu$ experiments in the foreseeable future. Each of these diagrams are dominated by D_ν, either due to high suppression scales as in the case of $\mathcal{O}_7$ and $\mathcal{O}_8$, or, as in $\mathcal{O}_{35}$ and $\mathcal{O}_{58}$, the operator's fermion content simply disfavors other contributions to the $\beta\beta0\nu$ amplitude. It is the general form of the neutrino-mass matrix derived in Table I, where we see that $m_{ee} \propto y_e$, that drives these operators away from their peers near $m_{ee}^{\rm eff} = 0.05$ eV. It is unfortunate that the two "low" dimensionality operators $\mathcal{O}_7$ and $\mathcal{O}_8$ are cut off by energy scales Λ_ν in excess of 100 TeV and are hence invisible to any direct probe. If either of these operators has anything to do with nature, it is unlikely that LNV will be observed in the foreseeable future in *any* experiment. On the other hand, any observation of LNV will rule out these types of scenarios. Additionally, as will become clear shortly in Sec. IV, current neutrino oscillation data already marginally disfavor such operators and have ample room to tighten constraints in the near future.

It is interesting to point out that the lower boundary of the currently excluded region falls within the $m_{ee}^{\rm eff}$ distribution, suggesting exciting prospects for the future. That being said, one should not read too much into current and future null results as, for most operators, relatively small cancellations and order one factors, not accounted for here, can push the relevant rates below the observable level depending on the underlying ultraviolet theory. On the other hand, one is allowed to interpret that operators that lead to $m_{ee}^{\rm eff} \gtrsim 10$ eV are severely constrained (if not ruled out) as proper explanations for neutrino masses if one assumes the new physics to be flavor "indifferent"—order one factors cannot be evoked to save the scenario. Once this assumption is dropped, however, it is quite easy to "fix" these scenarios, since the large $\beta\beta0\nu$ rate is a direct

[9]As it turns out, these are all suppressed by a single bottom quark Yukawa coupling as well as two powers of the $SU(2)_L$ gauge coupling g, but this fact cannot be deduced from Fig. 4 alone.

consequence of the universal order one couplings and the relatively low cutoff energy scale Λ_ν. For example, one can suppress the coupling of new physics to first generation fermions (compared to second and third generation fermions), thereby suppressing the worrisome diagrams of Fig. 3. This will have little effect on the relation between Λ and the neutrino masses, discussed in Sec. II, since these are either generation independent or highly reliant on third generation Yukawa couplings. Of course, by combining $\beta\beta0\nu$ searches with other probes we can obtain a much better idea of the origins of LNV as well as the relevant model(s), if any, chosen by nature.

B. Other rare LNV decay processes

Most of the qualitative discussions of Sec. III A, devoted to $\beta\beta0\nu$, can be directly applied to other rare decay processes with the same underlying kernel interaction described by Eq. (3.1). For such processes one need only analyze simple variants of the diagrams listed in Fig. 3, using crossing amplitude symmetries to account for the needed initial- and final-state fermions. Other factors must be added to the various electroweak vertices to account for quark-flavor mixing. The requisite CKM matrix elements can highly suppress many diagrams for processes involving cross-generational quark couplings. In fact, only tree-level D_9 diagrams are safe from such suppressions. Next, and most importantly, one must include the appropriate characteristic momentum transfer Q of the new system. Specific rates are highly dependent on this quantity as effective operator cross sections typically grow with some power of Q. The particular exponent of the power law depends on the diagram, but naive dimensional analysis dictates that $\Gamma \propto Q^{12}$ for diagram D_9, rendering it highly dependent on a reaction's energy transfer. The fact that each diagram varies with Q in a different way implies that predicting the dominant contributions to a given process is nontrivial and must be addressed quantitatively. Finally, in the cases of hadronic decays, one must also account for initial/final-state matrix elements. We assume that all factors can be simply estimated on dimensional grounds.

Unlike the $\beta\beta0\nu$ case, some meson decay modes proceeding via new LNV tensor interactions are expected to be suppressed. Such processes are one instance in our analysis where an operator's Lorentz structure can qualitatively affect expected LNV decay rates. One can understand this by considering a meson decay mediated by a new tensor particle. The parton-level interaction has the form $(\bar{u}\sigma_{\mu\nu}d)T^{\mu\nu}$ where the initial-state quarks are explicitly shown and all other fields are contained in the tensor $T^{\mu\nu}$. Following the standard procedure we factor out the hadronic structure in the form of a free decay constant and write the amplitude as generally allowed by Lorentz invariance in terms of the external state's four-momentum. Because of the antisymmetry of $\sigma_{\mu\nu}$, this amplitude vanishes to first order. Nonzero contributions to this decay mode must necessarily involve individual parton momenta and are therefore suppressed relative to the usual vectorlike decay calculations. From this, it is clear that models of LNV containing tensor couplings will often evade the predictions and bounds of this section. Tensor operators will mediate LNV meson decays into more complicated final states (one may include, say, initial/final-state radiation). Associated rates are, however, subject to additional gauge coupling and phase space suppression that tend to further reduce the already tiny LNV rates beyond any hope of detection.

Rare LNV meson decays have been experimentally pursued for many years [17]. Here, we focus on the $\Delta L = 2$ processes $M' \to M + \ell_\alpha^\pm \ell_\beta^\pm$, where M' and M are the initial- and final-state mesons, respectively, and the ℓ's represent like-sign lepton pairs of arbitrary flavor. Electric charge conservation dictates that M' and M have equal and opposite charge. Here we take each meson to consist of a color singlet up-type/antidown-type bound state[10] and factor out all long distance hadronic effects. In this way we can view the meson decay process as $d\bar{u} \to \ell_\alpha \ell_\beta + \bar{d}u$ for all up-type and down-type quark-flavor combinations. The effective LNV diagrams contributing to this process are shown in Fig. 5 with the same naming scheme as their analogs in Fig. 3. Here, V and V' denote potentially distinct elements of the quark mixing matrix. We additionally point out the potential dependency on all entries of the Majorana neutrino-mass matrix elements $m_{\alpha\beta}$ in diagram D_ν, as opposed to the $\beta\beta0\nu$ case where D_ν depends only on m_{ee}. These processes probe combinations of the neutrino masses that are naively unconstrained by $\beta\beta0\nu$ [28]. In general, the varied flavor structures encountered in meson decays allow for experimental probes into new physics couplings across the fermion generations. We pointed out earlier that some of the LNV operators lead to unacceptably large rates for $\beta\beta0\nu$ unless first generation quarks participate in the new interactions with severely suppressed couplings (compared with second and third generation quarks). If such a scenario is realized in nature, rare D or B decays may be much more frequent than naive expectations. For this reason, improving rare decay sensitivities to all channels is essential to completely constrain models of new LNV physics beyond the minimal framework analyzed here.

Reference [16] summarizes LNV upper bounds on all of these processes in terms of the effective Majorana neutrino-mass matrix element $m_{\alpha\beta}^{\text{eff}}$ that one would extract from observation assuming that all decay rates are dominated by the light neutrino exchange shown in D_ν. Hence,

[10]For simplicity, we assume that both the process $M' \to M + \ell_\alpha \ell_\beta$ and its conjugate have similar amplitudes and therefore we treat them symmetrically. Large CP-violating effects can invalidate this assumption.

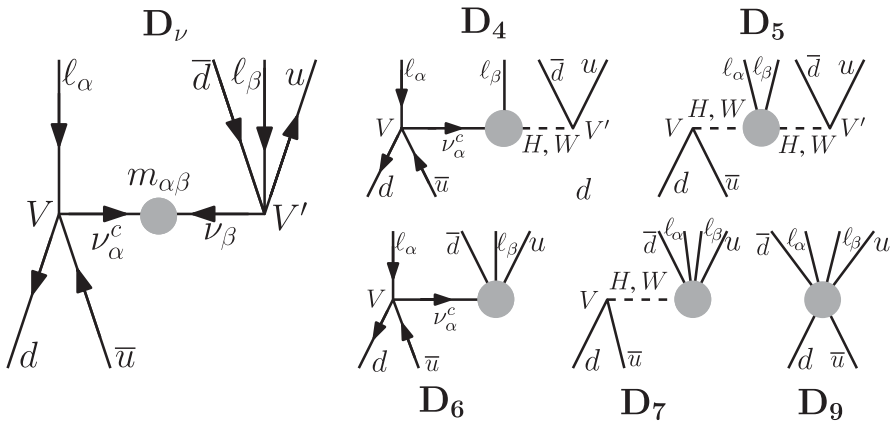

FIG. 5. The parton-level Feynman diagrams contributing to rare LNV meson decay labeled by the dimension of the underlying lepton number violating interaction, indicated by gray dots. Each diagram is generated, at some order in perturbation theory, by all analyzed interaction, but estimates of their magnitudes depend heavily on the details of the operators, including their associated scale Λ_ν, fermion content, and helicity structure.

we can compare operator expectations with current experimental limits in exactly the same way as was done in Sec. III A. For a given LNV meson decay, $m^{\rm eff}_{\alpha\beta}$ is defined from the contribution of the different classes of diagrams to the rare meson decay in question, exactly as $m^{\rm eff}_{ee}$ was defined in the previous subsection [see Eqs. (3.3) and (3.4)]. Direct estimates for different processes reveal $m^{\rm eff}$ distributions similar to that for $m^{\rm eff}_{ee}$ depicted in Fig. 4, up to "rescalings" that reflect the different kinematics and the presence of small CKM mixing matrix elements. Results are summarized in Fig. 6 for a representative sample of charged meson decays. Each histogram is labeled by its associated decay mode and is color-coded to indicate the neutrino-mass constrained cutoff scale Λ_ν of the different

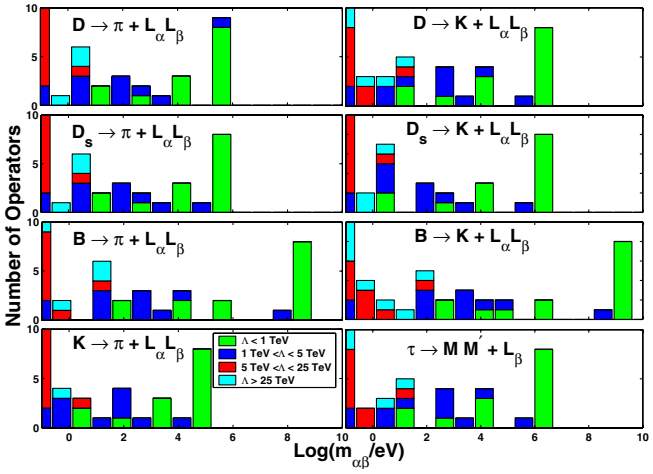

FIG. 6 (color online). $m^{\rm eff}_{\alpha\beta}$ distribution for several rare LNV meson and τ decays. Calculations assumed the charge lepton flavors $\ell_\alpha\ell_\beta = \mu e$, while the τ decay histogram (lower right-hand panel) was obtained assuming the final-state mesons $MM' = KK$. The histogram bars are color-coded by suppression scale. Current bounds on these processes are typically above 1 TeV and are not visible at these small scales.

LNV effective operators. For simplicity, we refrain from listing operator names on the individual histogram bars (as opposed to what was done in Fig. 4). The "operator ordering" is very similar to that of Fig. 4, especially in the low Λ_ν scale, high effective mass regime where decay rate predictions are particularly important. Note that the horizontal axes are relatively fixed for easy comparison and that the vertical direction is truncated and does not reflect the true "height" of the lowest mass bar (order 100 operators).

Specifically, we present effective Majorana neutrino-mass distributions for the processes, reading down the panels from left to right, $D \to \pi + \ell^\pm_\alpha \ell^\pm_\beta$, $D \to K + \ell^\pm_\alpha \ell^\pm_\beta$, $D_s \to \pi + \ell^\pm_\alpha \ell^\pm_\beta$, $D_s \to K + \ell^\pm_\alpha \ell^\pm_\beta$, $B \to \pi + \ell^\pm_\alpha \ell^\pm_\beta$, $B \to K + \ell^\pm_\alpha \ell^\pm_\beta$, $K \to \pi + \ell^\pm_\alpha \ell^\pm_\beta$, as well as the rare τ decay, $\tau^\pm \to MM' + \ell^\mp_\beta$.[11] Here the final-state leptons can be of any flavor allowed by energy conservation. Since, as previously discussed and explicitly verified numerically, the specific details of the distributions are mainly dictated by kinematics and CKM matrix elements, these results are robust under changes in the final-state lepton flavors. The τ decay distribution shown in the lower right panel is representative of all possible decay products including first and second generation charged leptons and light meson states. One should notice the expected general operator trend within each histogram as the characteristic cutoff scale is decreased, as well as the expected peaks near 0.05 eV dominated by light Majorana neutrino exchange. Additionally, each distribution is much "broader" than the one in Fig. 4. This observation exemplifies the fact that effective mass calculations depend critically on the underlying process. Indeed, maximum $m^{\rm eff}_{ee}$ values can reach

[11]The actual calculations displayed in Fig. 6 assumed the charge lepton flavors $\ell_\alpha\ell_\beta = \mu e$, while the τ decay histogram (lower right-hand panel) was produced assuming the final-state mesons $MM' = KK$.

nearly 10^{10} eV for the $B^+ \to K^- + e^+e^+$ decay but only 10^3 eV for $\beta\beta0\nu$. Current upper bounds for $m^{\rm eff}$ from these processes, mostly well above 1 TeV, are well beyond the largest operator predictions here, ranging from $m^{\rm eff}_{e\mu} < 0.09$ TeV for the case of $K^+ \to \pi^- e^+ \mu^+$ to $m^{\rm eff}_{\mu\mu} < 1800$ TeV for the case of $B^+ \to K^- \mu^+ \mu^+$ [16]. It is curious that the best meson decay bounds come from the rare LNV kaon process but, as can be seen in the lower left panel of Fig. 6, these yield by far the lowest predictions. Even provided vast improvements in meson production luminosities, future experiments will only have the potential to probe a few, select operators. Current and upgraded B factories [29] are expected to provide the most significant improvements, considering the large derived B-meson effective masses shown in Fig. 6. Still, the best cases from the figure yield only the tiny branching fraction 1.8×10^{-17} for the case of the rare decay $B^+ \to \pi^- e^+ \mu^+$, nearly 11 orders of magnitude below the current experimental limit of 1.3×10^{-6} [17].

Another possible search mode involves the decay of the Z boson into LNV final states. The dominant contributions to this process are generally unrelated to the reactions summarized in Eq. (3.1) and shown schematically in Figs. 3 and 5. While there is a slight connection between them as one can always attach a Z boson to various fermion lines in each diagram, there are potentially large lower order contributions arising within the operators themselves. The latter, when present, can easily overtake the associated ''golden mode'' counterparts. In this context, such processes can be thought of as the decay of the longitudinally polarized Z boson. Strict bounds exist on such decays from the LEP-I [30] and SLAC Large Detector [31] experiments. Each element of the operator set predicts decays into final-state fermions with total lepton number $L = 2$. The dilepton pair can be of any flavor and is generally accompanied by two or four additional fermion states, depending on the dimension of the operator. We restrict our discussion to the dimension-11 operators comprising the majority of the sample, as these are typically suppressed by lower cutoff Λ_ν scales and, equally important, explicitly contain Higgs doublets in their field content. In this case, tree-level decays result in a six-fermion final state which suffers from a large phase space suppression and cumbersome multiplicities that are likely to render even the most sophisticated search ineffective. The only possibility of this type that yields a charged dilepton signal is $Z \to \ell^\pm_\alpha \ell^\pm_\beta q\bar{q}q\bar{q}$ (quarks of all allowed flavors implied), but many other possibilities exist involving invisible final-state neutrinos. A little thought also reveals that closing fermion loops in an attempt to obtain simpler final states and thus render the analysis more tractable will necessarily result in final-state neutrinos. Therefore, the majority of the Z-boson LNV decay channels involve invisible final states with practically undetermined total lepton number. The prospect of direct discovery by these means seems dismal, but indirect constraints on LNV are still possible from bounds on the Z-boson invisible decay width. There is currently a statistically insignificant, but nonetheless captivating, 2σ deviation between the observed invisible decay width and SM expectations assuming three light neutrino species [17]. The experimentally extracted branching ratio was found to be slightly *smaller* than its predicted value so that a new LNV contribution of the form $Z \to \nu_\alpha \nu_\beta$ would push the invisible branching ratio in the ''wrong'' direction. From these bounds the decay width of any new contribution to the Z-boson decay is constrained to be less than 2.0 MeV at the 95% confidence level [17,32]. A quick estimate reveals that this constrains the dominant LNV amplitudes $A_Z < \sqrt{4\pi(2.0\ {\rm MeV}/M_Z)} \sim 0.53$. For the dimension-11 operators of interest, the largest possible amplitude is of order $y^2/(16\pi^2)^2(v/\Lambda)^3$ where y is an arbitrary fermion Yukawa coupling and four powers of the cutoff scale Λ are removed by divergences in the closed diagram loops. The constraint above translates into $y^2(v/\Lambda)^3 < 4.1 \times 10^2$, which is easily evaded by even the best case scenario of $y = y_t \approx 1$ and $\Lambda \approx v$. Experimental bounds on $\Gamma_{\rm inv}$ must be improved by a factor of a million before they start significantly constraining LNV (under the assumptions made here). This result holds for virtually all possible flavor structures. We conclude that rare Z-boson decays are not practical discovery modes for the LNV effects considered here, but look to future rare Z-boson decay studies for more information.

In a similar way, one can also dismiss the case of rare W-boson decays as promising probes of LNV. As in the Z-boson case, the W boson can decay into a variety of $L = 2$ final states proceeding either through couplings to left-handed fermion lines or explicit operator content. Here, however, there is no six-fermion, same-sign dilepton final state with no neutrinos due to conservation of charge and weak isospin, so the lowest order observable mode is already loop suppressed to $W^- \to \ell^-_\alpha \ell^-_\beta + q\bar{q}$. Current W-boson decay bounds are far too weak to constrain such suppressed LNV [17] and are not likely to improve to the level implied by the operators under consideration, which predict the tiny decay rate $\Gamma_{\rm LNV} \leq m_W(4\pi)/(16\pi^2)^5(v/\Lambda)^{10} \approx 10^{-5}$ MeV in the best case scenario of electroweak scale Λ_ν. We also point out that, contrary to the Z-boson decay limits, there are no robust, indirect bounds that can be used to constrain LNV in the case of the W boson. Note that, despite dismal prospects for gauge boson decay driven LNV discovery within the minimal framework of ''natural'' effective operators, one can still construct theoretically well-motivated models that will yield observable signals. Particularly, in a weak-scale seesaw mechanism ($\mathcal{O}_1$), the new degrees of freedom, comprised mostly of Majorana gauge singlet fermions (right-handed neutrinos), can mediate visible, $\Delta L = 2$, W-boson mediated processes with little or no scale/loop

suppression. This class of model is analyzed in [33] and is exempt from the discussion outlined here.

C. Collider LNV signatures

If neutrino masses are a consequence of ultraviolet physics related to cutoff scales around the TeV scale, we expect future high-energy collider searches to directly access the new LNV physics. For example, the direct, resonant production of new states could lead to rather spectacular signals of these models. It would also indicate the breakdown of the effective field theory approach undertaken here. To pursue such possibilities, one must assume a specific ultraviolet sector and study its signatures and implications on a case-by-case basis. In the looming shadow of the LHC [34] and the more distant ILC [35], such an analysis is highly warranted but will not be pursued here. Instead, we assume that the masses of new ultraviolet degrees of freedom remain out of the reach of next-generation accelerator experiments. Such a situation can be easily accommodated within the context of the preceding results, considering the order of magnitude nature of the Λ_ν estimates.

We will concentrate on the process $e^-e^- \to q\bar{q}q\bar{q}$ (which will usually manifest themselves as jets) with no missing energy in an ILC-like environment [35] with a center-of-mass energy of 1 TeV and an integrated luminosity of 100 fb^{-1}. We also make the oversimplifying assumption that the detector system has equal acceptance to all quark flavors, and the ability to efficiently distinguish quarks, gluons, and τ's. By summing over all possible quark final states it is simple to estimate the total LNV cross section for each effective operator, assuming it is responsible for neutrino masses. Such searches can be complemented by looking at $e^-e^- \to W^-W^-$, which have been discussed in detail in the literature [36]. As discussed in Sec. III B, the different LNV operators couple to one or more gauge bosons via an appropriately closed fermion loop or direct coupling to the Higgs doublet field.

Charge and baryon number conservation dictate that the two quarks in $e^-e^- \to q\bar{q}q\bar{q}$ are down-type quarks, while the two antiquarks are up-type antiquarks. At the parton level, the scattering process is similar to $\beta\beta0\nu$, which motivates exploiting simple variations of the diagrams in Fig. 3 in order to calculate the relevant amplitudes, as was done in Sec. III B. Here, the extensions are obvious: use crossing symmetry to rotate all lepton lines into the initial state and all quark lines to the final state taking special care to insert appropriate CKM matrix elements where needed. Because of the large characteristic momentum transfer Q of the e^-e^- scattering, one must also "expand" the electroweak vertices and account for gauge boson propagation. With this in mind, the amplitude calculations can be carried over directly from the previous sections. Specific results are, however, quite distinct due to the higher center-of-mass energies involved. In the language of the underlying diagrams mediating this reaction, for diagrams characterized by TeV cutoff scales, diagram D_9, if allowed at tree level, will dominate the rates. As in the previous cases, for intermediate to high cutoff scales, general diagram dominance must be addressed on a case-by-case basis. It is important to appreciate that, since these are nonrenormalizable effective interactions, cross sections grow with center-of-mass energy. For this reason, we expect many of the low cutoff scale operators to yield observably large signals at the ILC.

Figure 7 shows the $e^-e^- \to q\bar{q}q\bar{q}$ cross-section distribution, in femtobarns, at the ILC, calculated for all 129 of the analyzed LNV operators. Once again, the extracted value of the cutoff energy scale Λ_ν assuming constraints from neutrino masses are color-coded to indicate operators associated with a low ($\Lambda_\nu \lesssim 10$ TeV) or high ($\Lambda_\nu \gtrsim 10$ TeV) ultraviolet cutoff. Each bar is also labeled with the respective constituent operators, for convenience. Note that the vertical axis is truncated at 15 operators (the leftmost bin is over 60 operators high) to help clearly display relevant features of the plot. We also highlight the potential reach (defined as a cross section greater than the inverse of the integrated luminosity) of the ILC with a broken vertical line, assuming 100 fb^{-1} of integrated luminosity. This particular ILC luminosity value should be considered as a loose lower bound, introduced to give a feeling for the observable scales involved. It has recently been argued, for example, that a realistic machine should be able to outperform this estimate by over an order of magnitude [35].

A glance at Fig. 7 reveals that it generally adheres to the expected correlation of decreasing Λ_ν scales with increasing LNV rates, similar to what is observed for other LNV

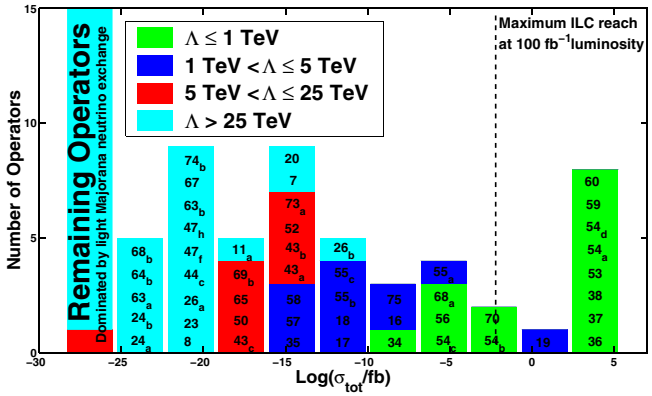

FIG. 7 (color online). Distribution of total cross section for the process $e^-e^- \to q\bar{q}q\bar{q}$ and no missing energy at an e^-e^- collider with 1 TeV of center-of-mass energy. Estimates were obtained assuming the scales Λ_ν derived in Sec. II, as well as order one coupling constants. The histogram bars are labeled with operator names and color-coded by the Λ_ν cutoff scale. Also shown (broken vertical line) is the reach of such an experiment assuming 100 fb^{-1} of integrated luminosity. The vertical axis is truncated to best display the relevant features of the plot.

observables (e.g., Fig. 4). The similarities between the different processes extend beyond mere trends to the specific ordering of the operators within each histogram. This reflects the common underlying interactions that drive these processes. The operators on the far right of the plot, topping off the highest cross sections, are exactly those operators with the largest m_{ee}^{eff}, now "split" into three different bars. The large bar just below 10^5 fb is composed of sub-TeV scale operators with tree-level diagram D_9-like fermion content. Slightly smaller are the expectations for $\mathcal{O}_{19}$, again dominated by diagram D_9, but characterized by a slightly larger Λ_ν scale (around 1 TeV). Moving down in cross section, this is followed by the low cutoff scale operators $\mathcal{O}_{54_{b,c}}$ and $\mathcal{O}_{70}$, dominated by a combination of diagrams D_6 and D_7. On the opposite end of the plot we point out the large bar below 10^{-25} fb, composed mainly of operators associated with high cutoff scales ($\Lambda_\nu > 25$ TeV). The contributions of these operators are dominated by light Majorana neutrino exchange, but their histogram bars contain far fewer models than their $\beta\beta0\nu$ counterpart, as many of the latter have been driven up due to new diagram D_4 and D_5 contributions. In general, the large center-of-mass energies tend to magnify differences between interaction rates that were not relevant in low-energy observables. This naively suggests that high-energy probes have a higher potential for distinguishing different models.

There are 11 operators that lead to an observably large (as defined earlier) $e^-e^- \to q\bar{q}q\bar{q}$ cross section at the ILC. Note that all of these were already "ruled out" by current $\beta\beta0\nu$ searches. As discussed in Sec. III A, however, these bounds only effectively limit the couplings of the new physics to the first generation of quarks and leptons, and hence, if such a scenario is realized in nature, one should still expect large contributions from decay modes that lead to second and third generation final-state quarks. In fact, even one such heavy quark is enough to bypass the constraints from $\beta\beta0\nu$ for several effective operators. Such reasoning implies that constraints on the new physics flavor structure can be made quite strong at a linear collider via analyses of the flavor of the final-state quarks. By identifying and comparing the outgoing quark flavor, one can extract individual limits on quark-lepton coupling constants within the operators. Additionally, kinematics can be used as a further operator probe. For example, one can potentially determine the dominant underlying LNV diagram (say D_6, D_7, or D_9) by checking whether the various kinematic distributions are characteristic of W-boson exchange.

The ILC can cleanly select or discard some LNV scenarios. This characteristic is further enhanced by considerations of initial electron polarization. Planned linear colliders have the ability to produce partially polarized beams (80% polarization for e^-, 40% for e^+ [35,37]). The power of a high-energy polarized e^-e^- beam is in model identification and rejection. Of all operators that yield observably large cross sections, the $e_L^-e_L^-$ mode can only probe $\mathcal{O}_{53}$, and therefore any positive LNV signal cleanly identifies this as the operator chosen by nature. In a similar way, the ILC running in its $e_L^-e_R^-$ mode can easily observe LNV from $\mathcal{O}_{19}$, $\mathcal{O}_{54_a}$, $\mathcal{O}_{54_d}$, $\mathcal{O}_{59}$, and $\mathcal{O}_{60}$; and to a lesser extent, operators $\mathcal{O}_{54_b}$ and $\mathcal{O}_{70}$, and possibly even $\mathcal{O}_{54_c}$. Finally the $e_R^-e_R^-$ mode can probe operators $\mathcal{O}_{36}$, $\mathcal{O}_{37}$, and $\mathcal{O}_{38}$. Within this framework, any LNV detected in one ILC polarization mode will generally not be seen in the others. This statement also applies to resonantly enhanced low scale operators that lie outside the observability window.

While e^-e^- collisions only probe effective operators that "talk" to first generation leptons, there are several lepton collider processes that allow one to explore other members of the charged-lepton family. Future high-energy muon colliders [38] could, in principle, also be used to study LNV. In this case, all of the preceding discussions regarding the ILC are applicable. Electron linear collider facilities can also be used to study γe^- and $\gamma\gamma$ collisions [39]. γe^- collisions can be used to probe $\gamma e^- \to \ell_\alpha^+ + X$ (and hence the "$e\alpha$" structure of different LNV operators), while $\gamma\gamma \to \ell_\alpha^\pm \ell_\alpha^\pm + X$ probes all the different α, β charged-lepton flavors. For $\gamma\gamma$ collisions, for example, considering projected ILC-like collider parameters, one would expect the same operator distribution as Fig. 7, shifted down in cross section by, roughly, a factor of $\alpha^2 \sim 10^{-4}$. Thus, a handful of operators should be testable at a future $\gamma\gamma$ collider assuming 100 fb^{-1} of integrated luminosity.

The preceding analyses carry over to the case of hadron colliders, such as the LHC, in a relatively straightforward way. The LHC, or Large Hadron Collider, is a proton–proton machine that will operate at a center-of-mass energy of 14 TeV and a characteristic integrated luminosity around 100 fb^{-1} [34] (in its high luminosity mode). The relevant LNV variants of Eq. (3.1) are $dd \to \ell_\alpha^-\ell_\beta^- uu$ and $uu \to \ell_\alpha^+\ell_\beta^+ dd$ with no missing energy. Of course, at center-of-mass energies well above a TeV, the proton–proton collisions are dominated by the gluon content of the proton, so most interactions at the LHC will be initiated by gluon–gluon and gluon–quark scattering. The dominant LNV subprocesses are $qg \to \ell_\alpha^\pm \ell_\beta^\pm q\bar{q}q$ and $gg \to \ell_\alpha^\pm \ell_\beta^\pm q\bar{q}q\bar{q}$ and are illustrated in diagrams (a) and (b) of Fig. 8, respectively. These are characterized by similar final states as the quark–quark scattering reactions but, given that there is no explicit gauge boson field content in the LNV operators in question (Table I), their amplitudes are proportional to unimportant order α_s and α_s^2 coefficients, respectively. The parton-level diagram (c) shows the related process $gg \to \ell_\alpha \nu_\beta + q\bar{q}$. The rate for this process can be estimated, relative to its four jet cousins, by exchanging a final-state phase space suppression for a single loop suppression. In all three diagrams depicted in

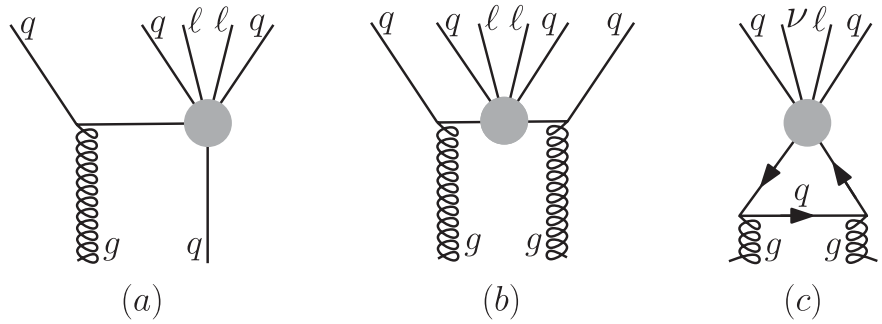

FIG. 8. Parton-level gluon–gluon and gluon–quark LNV interactions relevant at high-energy hadron colliders. Each of these yields a same-sign dilepton signal with jets and no missing energy. Notice that the final-state flavor structure is completely arbitrary under the assumption of random order one coupling constants.

Fig. 8, the LNV interaction regions represented by large gray dots contain all of the diagrams discussed earlier, meaning that the operator amplitudes calculated for the ILC can be recycled in this analysis. While all three bare diagrams are characterized by rates of the same order of magnitude, diagram (c) leads to missing transverse energy and potentially undetermined final-state lepton number, rendering it a less than optimal experimental search mode. Note that, in all of these cases, the external, and internal, fermions outside of the LNV interaction region can be of any flavor. Therefore, hadron collider experiments have, in principle, access to *all* LNV operator parameters. Cleanly identifying and constraining all said parameters should prove quite difficult for all but the most obvious signatures. The above statements regarding signals at the LHC are also applicable at the Tevatron with some minor, but important, modifications. The Tevatron's $p\bar{p}$ collisions are at a much lower center-of-mass energy, roughly 2 TeV, while the total expected integrated luminosity, less than 10 fb^{-1} per experiment, is orders of magnitude smaller. These factors lead to much lower amplitudes, reduced by approximately a factor of $(Q_{\text{Tevatron}}/Q_{\text{LHC}})^5 \approx 10^{-5}$ |.[12] The smaller center-of-mass energy also limits the Tevatron's ability to directly produce new physics states. With this in mind we conclude that the Tevatron has little or no chance of discovering LNV (within this minimal framework).

A detailed set of predictions for the LHC would require a much more refined analysis, including the effects of parton structure functions, flux distributions, and backgrounds, and as such is beyond the scope of this general survey. We would, however, like to point out that some of the reactions outlined here are subject to large background rates. While SM processes are lepton number conserving, many can fake the LNV signals in the complicated environment of a high-energy hadronic interaction. The requirement of no missing final-state energy is particularly hard to accommodate as some energy is always lost down the beampipe. As is typically done, one must rely on the less restrictive conservation of transverse momentum in order to constrain invisible states, such as neutrinos. SM same-sign dilepton production processes arising from, say, W-boson pair production are serious potential sources of background. Furthermore, it is impossible to predict correlations among final-state jets without selecting a particular operator and underlying model of new physics, making it difficult to impose general cuts to reduce other hadronic backgrounds. Of course, some of the low scale LNV operators yield large enough total cross sections that even crude analyses may suffice to reveal their existence. We conclude by pointing out that a large amount of recent work has been dedicated to LNV searches at collider facilities [40]. Most of these approach the subject from the perspective of sub-TeV mass, mostly sterile Majorana neutrinos that mix with the active neutrinos and are thus related to light neutrino masses via the seesaw mechanism [9]. This amounts to one example that leads to the dimension-five operator $\mathcal{O}_1$, but where one assumes that the propagating degrees of freedom are 12 or 13 orders of magnitude lighter than the ultraviolet cutoff scale Λ_ν.[13] In this case, LNV interactions are dominated by diagram D_ν of Fig. 3 [where heavy (weak-scale) neutrinos are also exchanged], and as such one should make use of specific kinematic cuts to reduce background rates. These cuts, however, may also remove LNV signals resulting from many of the scenarios explored here, particularly those whose rates are dominated by D_9 at tree level. We urge experimentalists to account for this possibility while analyzing future data sets.

[12]Strictly speaking, one must also account for the proton's structure functions at the Tevatron's energy scale. Unlike the LHC, where collisions are dominated by gluon–gluon interactions, proton collisions at the Tevatron are dominated by valence quark interactions. These considerations do not affect our conclusions.

[13]This can be achieved in two different ways. Either the new physics is very weakly coupled, or the combined new physics and SM couplings are finely tuned [14]. In order to observe right-handed neutrinos in colliders, the latter must be realized.

IV. NEUTRINO MIXING

Table I contains predictions for *all* the entries $m_{\alpha\beta}$, of the Majorana neutrino-mass matrix. These are computed in the weak basis where the weak interactions and the charged-lepton Yukawa couplings are diagonal, so that the eigenvalues of the neutrino-mass matrix are the neutrino masses (bounded by oscillation experiments and, say, precision measurements of tritium beta-decay [7]), while its eigenvectors determine the neutrino mixing matrix, constrained mostly by oscillation experiments. Since different LNV effective operators predict different flavor structures for the neutrino-mass matrix, there is the possibility to constrain the different scenarios with existing oscillation data [3]. While we can only predict the values of $m_{\alpha\beta}$ within, at best, an order of magnitude, it is still possible to extract useful information from the derived large scale structure of the expressions. In particular, we can test the hypothesis of whether λ values associated with different lepton flavors are allowed to be of the same order of magnitude. In order to obtain more accurate predictions and further probe the fine details of lepton mixing, one must succumb to specific models, beyond the scope and philosophy of this analysis.

The mass matrix for the three light Majorana neutrinos can be reconstructed from nine observables: three masses m_1, m_2, m_3, taken to be real and positive; three (real) mixing angles θ_{12}, θ_{23}, θ_{13}; and three CP-violating phases δ, ϕ_3, ϕ_2. Here, δ is a so-called Dirac phase that is generally present in the system regardless of the neutrino's nature (Majorana or Dirac fermion), while ϕ_1, ϕ_2 are the so-called Majorana phases, only present if the neutrinos are Majorana particles (which is the case of all scenarios under consideration here). Oscillation data determine with relatively good precision θ_{12}, θ_{23}, $\Delta m^2_{12} \equiv m_2^2 - m_1^2$, and $|\Delta m^2_{13}| \equiv |m_3^2 - m_2^2|$. We define neutrino masses such that $m_1 < m_2$ and $\Delta m^2_{12} < |\Delta m^2_{13}|$, so that the sign of Δm^2_{13} remains as an observable that characterizes the neutrino-mass hierarchy ("normal" for $\Delta m^2_{13} > 0$, "inverted" for $\Delta m^2_{13} < 0$). See, for example, [1] for details. As for the third mixing angle, $\sin^2\theta_{13}$ is constrained to be less than 0.025 (0.058) at 2σ (4σ) from a three neutrino global oscillation analysis [3]. A considerable amount of uncertainty remains. In particular, we have only upper bounds on the absolute neutrino-mass scale, from kinematical measurements such as tritium beta decay [4,5], plus cosmological observations [6]. Finally, the three CP violating phases are completely unconstrained, and we have no information regarding the neutrino-mass hierarchy.

The above experimental results allow for several different "textures" for $m_{\alpha\beta}$ in our weak basis of choice (see, for example, [41]). The purpose of this section is to discuss whether any of the textures predicted by the different LNV effective operators is "ruled out" by current observations. Most of the analyzed operators imply "anarchic" [8] neutrino masses. This simply means that all elements of the neutrino-mass matrix are uncorrelated and of the same order of magnitude. This hypothesis is known to "fit" the current data very well [8]. It will be further challenged by searches for θ_{13} (the anarchic hypothesis favors large θ_{13} values) and probes that may reveal if the neutrino masses are hierarchical or whether two or three of the masses are almost degenerate (anarchy naively predicts the former). If future data strongly point towards nonanarchic $m_{\alpha\beta}$, we will be forced to conclude that there is nontrivial "leptonic" structure in the dimensionless coefficients λ of most of the LNV operators considered here.

Many of the operators associated with a low neutrino-mass related cutoff scale ($\Lambda_\nu \leq 10$ TeV), on the other hand, naively predict more structured neutrino-mass matrices. Operators

$$\mathcal{O}_7,\ \mathcal{O}_8,\ \mathcal{O}_{19},\ \mathcal{O}_{20},\ \mathcal{O}_{34},\ \mathcal{O}_{35},\ \mathcal{O}_{54_{a,b,c,d}},\ \mathcal{O}_{55_{a,b,c}},\ \mathcal{O}_{56},\ \mathcal{O}_{57},\ \mathcal{O}_{58},\ \mathcal{O}_{59},\ \mathcal{O}_{60},\ \mathcal{O}_{70},\ \mathcal{O}_{75}, \tag{4.1}$$

which radiatively generate neutrino-mass elements proportional to distinct charged-lepton Yukawa coupling (y_e, y_μ, y_τ), yield mass matrices m such that

$$m \propto \begin{pmatrix} y_e & y_\mu & y_\tau \\ y_\mu & y_\mu & y_\tau \\ y_\tau & y_\tau & y_\tau \end{pmatrix}. \tag{4.2}$$

Additionally, models described at low energies by $\mathcal{O}_{36}$, $\mathcal{O}_{37}$, and $\mathcal{O}_{38}$ generate neutrino masses proportional to both associated charged Yukawa couplings, such that

$$m \propto \begin{pmatrix} y_e y_e & y_e y_\mu & y_e y_\tau \\ y_e y_\mu & y_\mu y_\mu & y_\mu y_\tau \\ y_e y_\tau & y_\mu y_\tau & y_\tau y_\tau \end{pmatrix}. \tag{4.3}$$

The strongly hierarchial nature of the charged-lepton masses ($y_e \ll y_\mu \ll y_\tau$) implies that the $m_{\alpha\beta}$ elements of Eqs. (4.2) and (4.3) are expected to be hierarchical as well. In particular, the ee matrix element, m_{ee}, proportional to y_e or y_e^2 is, for all practical purposes, negligibly small[14] in both of these cases. On the other hand, it is well known that only a normal neutrino-mass hierarchy is consistent with vanishing m_{ee} [42], so that both Eqs. (4.2) and (4.3) predict the neutrino-mass ordering to be normal. In the absence of extra structure, scenarios characterized by the LNV operators listed in Eq. (4.1) plus $\mathcal{O}_{36}$, $\mathcal{O}_{37}$, and $\mathcal{O}_{38}$ will be ruled out if future data favor an inverted mass hierarchy, or if the neutrino masses end up quasidegenerate (regardless of the hierarchy). As will become clear shortly,

[14]Quantitatively, in the scenarios under investigation, m_{ee} values are, respectively, up to order one corrections, $y_e/y_\tau \sim 10^{-4}$ and $y_e^2/y_\tau^2 \sim 10^{-7}$ times the characteristic mass scale of the mass matrix.

Eqs. (4.2) and (4.3) predict that the lightest neutrino mass (m_1 in this case) is small ($\lesssim \sqrt{\Delta m^2_{12}}$).

A more detailed analysis reveals that naive expectations from Eq. (4.2) are already disfavored, while those from Eq. (4.3) are virtually excluded. Assuming the normal hierarchy and very small m_{ee}, one can find a relation between the neutrino-mass eigenstates and the oscillation parameters, thus reducing the number of free parameters in the mass matrix by 1. Consider the diagonalization of the neutrino-mass matrix defined by $m_{\alpha\beta} = UM^D U^T$ with $M^D = \mathrm{diag}(m_1, m_2 e^{2i\phi_2}, m_3 e^{2i\phi_3})$ and U the neutrino mixing matrix, expressed in the Particle Data Group parametrization. In this case,

$$m_{ee} = m_1 \cos^2\theta_{12}\cos^2\theta_{13} + m_2 \sin^2\theta_{12}\cos^2\theta_{13} e^{2i\phi_2} + m_3 \sin^2\theta_{13} e^{2i(\phi_3-\delta)}. \tag{4.4}$$

Setting $m_{ee} = 0$, one can solve for m_1 and one of the Majorana phases. Recalling that, for the normal mass hierarchy, $m_2 = \sqrt{m_1^2 + \Delta m^2_{12}}$ and $m_3 = \sqrt{m_1^2 + \Delta m^2_{13}}$, and assuming small θ_{13} and $\eta \equiv \sqrt{\Delta m^2_{12}/\Delta m^2_{13}}$,

$$\frac{m_1}{\sqrt{\Delta m^2_{13}}} \approx \eta \frac{\sin^2\theta_S}{\cos^{1/2}2\theta_S} - \theta^2_{13}\frac{\cos^2\theta_S}{\cos 2\theta_S}\cos[2(\phi_3-\delta)],$$
$$\phi_2 \approx \frac{\pi}{2} + \frac{1}{2}\arctan\left(\frac{4\theta^2_{13}}{\eta}\frac{\sqrt{\cos 2\theta_S}}{\sin^2 2\theta_S}\sin[2(\phi_3-\delta)]\right). \tag{4.5}$$

One can easily obtain approximate expressions for the other neutrino masses (m_2, m_3) and hence all elements $m_{\alpha\beta}$. Upon substituting the numeric best fit oscillation parameters to avoid introducing a needlessly cumbersome expression, we get

$$\frac{m_{\alpha\beta}}{\sqrt{\Delta m^2_{13}}} = 0.5 e^{i2\phi_3}\begin{pmatrix}0&0&0\\0&1&1\\0&1&1\end{pmatrix} + 0.71\theta_{13}e^{-i(\delta-2\phi_3)}\begin{pmatrix}0&1&1\\1&0&0\\1&0&0\end{pmatrix} + 0.45\eta\begin{pmatrix}0&-1.3&1\\-1.3&-1&0.61\\1&0.61&-0.36\end{pmatrix}$$
$$+ 0.91\theta^2_{13}\cos[2(\delta-\phi_3)]\begin{pmatrix}0&1&-0.89\\1&0.12&0.02\\-0.89&0.02&-0.12\end{pmatrix} + 1.2i\theta^2_{13}\sin[2(\phi_3-\delta)]\begin{pmatrix}0&1&-0.67\\1&1.2&-0.83\\-0.67&-0.83&0.56\end{pmatrix}. \tag{4.6}$$

Equation (4.6) suggests a clear hierarchy among the mixing matrix elements. The four, lower box-diagonal $\mu-\tau$ elements dominate, followed by the off-diagonal $e\mu$ and $e\mu$ entries, and finally the vanishingly small m_{ee}. Except for the vanishingly small m_{ee}, which was required *a priori*, all of the remaining properties follow directly from the experimentally determined mixing parameters. Among the dominant $\mu-\tau$ submatrix, Eq. (4.6) predicts that all entries are equal up to small order η and θ_{13} corrections. The magnitude, and sign, of these "breaking terms" can be tuned with the phases ϕ_3 and δ, and to a lesser extent by varying η and θ_{13} within their allowed ranges. On the other hand, the relative sizes of $m_{e\mu}$ and $m_{e\tau}$ are expected to be similar but not identical, i.e., $m_{e\mu} \sim m_{e\tau} \sim (m_{e\mu} - m_{e\tau})$.

While some of the gross features of Eq. (4.6) are shared by Eqs. (4.2) and (4.3), a finer analysis reveals several disagreements. The major discrepancy lies in the required relations among the matrix elements. Equation (4.2) predicts that all $m_{\alpha\tau}$ elements are equal, while Eq. (4.3) suggests $m_{e\tau} \ll m_{\mu\tau} \ll m_{\tau\tau}$. Both of these contradict, in different ways, the experimental constraint $m_{e\tau} \ll m_{\mu\tau} \approx m_{\tau\tau}$. Additionally, both Eqs. (4.2) and (4.3) predict $m_{ee} \ll m_{\mu\mu} \ll m_{\tau\tau}$, while observations require $m_{ee} \ll m_{\mu\mu} \approx m_{\tau\tau}$. Similarly, both sets of operators suggest $m_{e\mu} \ll m_{e\tau}$, while, experimentally, they are constrained to be similar.

In order to quantify how much Eqs. (4.2) and (4.3) (dis)agree with our current understanding of neutrino masses and lepton mixing, we numerically scanned the allowed mass matrix parameter space assuming the normal neutrino-mass hierarchy and constraining $|m_{ee}| \leq y_e/y_\tau \times 1\ \mathrm{eV} \approx 10^{-4}$ eV. It should be noted that, according to this relation, m_{ee} is allowed to deviate by nearly a factor of 10 above naive expectations from mass matrix Eq. (4.2), thus accounting for the possible order of magnitude uncertainties in operator scales and coupling constants. This feature is only included for completeness, as one expects that such m_{ee} excursions from zero will generally have a negligible effect on the mass matrix due to the robust nature of Eq. (4.6). Figure 9, a scatter plot of mixing matrix elements, depicts the result of such a scan. Note that we plot the mass ratios with respect to the assumed-to-be-dominant $m_{\tau\tau}$ element. The light gray regions of the plot were produced allowing all oscillation parameters to vary within their 95% confidence bounds [3] and phases to vary within their entire physical range subject to the constraints discussed above. In the purple (dark) region, the phases and reactor mixing angle θ_{13} are allowed to vary while all other

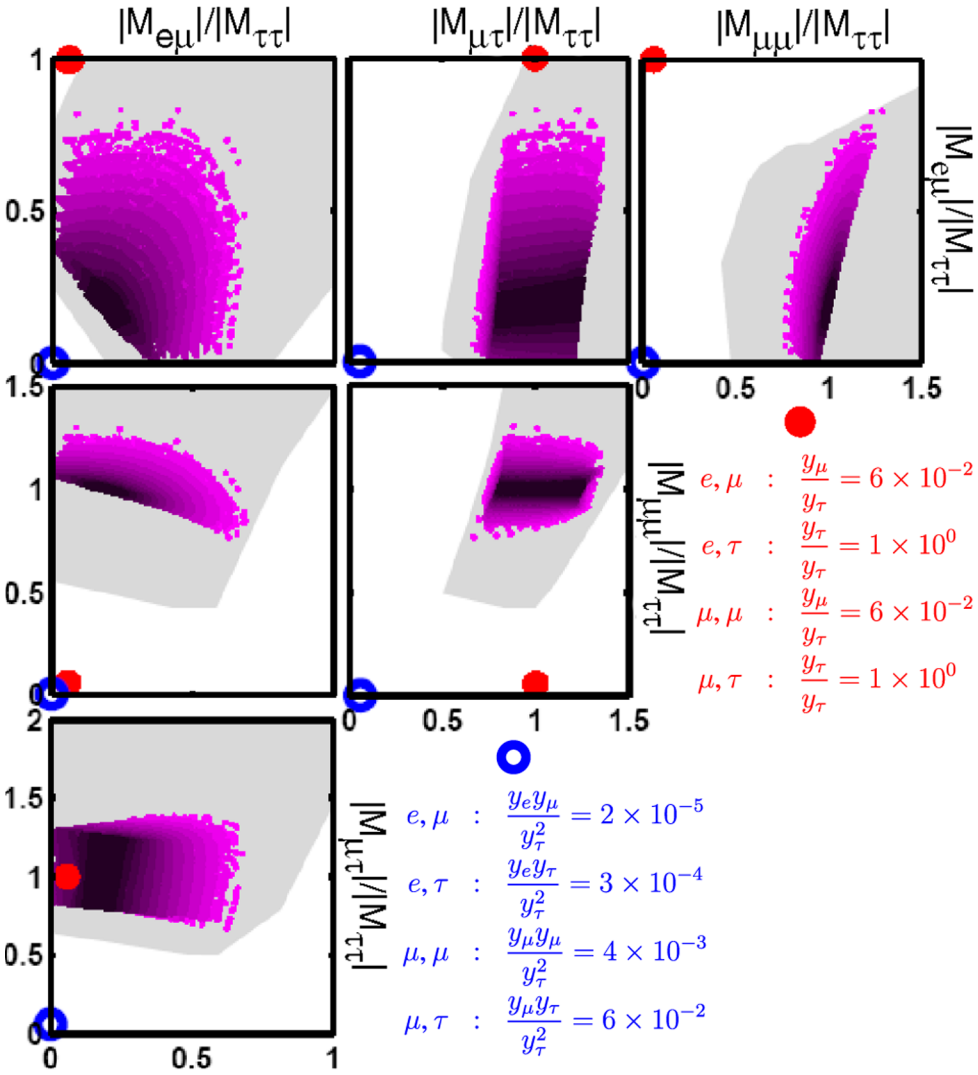

FIG. 9 (color online). Scatter plots of the symmetric Majorana neutrino-mass matrix elements normalized to $m_{\tau\tau}$. Each panel is produced assuming the normal mass hierarchy and parameter constraints insuring that $m_{ee} \leq 10^{-4}$ eV. The light gray region is calculated allowing all mixing parameters to vary within their respective 95% confidence intervals. In the purple (darker) regions, the solar and atmospheric parameters are held constant while all phases are scanned within their physical ranges and θ_{13} is varied between zero and its 4σ upper bound. The $\sin^2\theta_{13}$ variation is illustrated by varying the shading from dark to light. Also indicated by red (closed) and blue (open) dots are the expectations derived from Eqs. (4.2) and (4.3), respectively, along with a listing of their associated coordinate values.

mixing parameters are held fixed at their best fit values. We depict the $\sin^2\theta_{13}$ variation from zero to 0.06 (4σ upper bound [3]) by varying the purple shading from dark to light. It is easy to check that the numeric (Fig. 9) and analytic results [Eq. (4.6)] are consistent both qualitatively and quantitatively.

Figure 9 also depicts the predictions from Eqs. (4.2) and (4.3) with red (closed) and blue (open) dots, respectively. As expected, all the predictions from Eq. (4.3) fall near the origin in each panel and are safely excluded. Because expectations from Eq. (4.3) for all $m_{\alpha\beta}/m_{\tau\tau}$ are much smaller than 1, we also include the dot coordinate values for both textures within the figure. In order to render the neutrino-mass matrix predicted from $\mathcal{O}_{36}$, $\mathcal{O}_{37}$, and $\mathcal{O}_{38}$ consistent with experimental constraints on neutrino masses and lepton mixing, one is required to choose very hierarchical λ coefficients. In more detail, one needs to choose λ values so that all mixing matrix elements are enhanced relative to the dominant $m_{\tau\tau} \propto y_\tau y_\tau$ by numerical factors that range—for different entries—from 100 to 10^5. A possible mechanism for achieving this is to suppress third generation couplings to new physics, thus driving up the ratio $m_{\alpha\beta}/m_{\tau\tau}$ along with the required cutoff scale Λ_ν. This procedure would have to be accompanied by a more modest reduction of the couplings of second generation fermions. Basically, we need to impose a flavor structure that "destroys" the naive flavor structure induced by the charged-lepton Yukawa coupling hierarchy. We can safely

conclude that $\mathcal{O}_{36}$, $\mathcal{O}_{37}$, and $\mathcal{O}_{38}$, which suggest that the neutrino-mass matrix has the form Eq. (4.3), are strongly disfavored by current neutrino oscillation data and, if somehow realized in nature, must be accompanied by a very nontrivial flavor structure.

On the other hand, the operators listed in Eq. (4.1), which predict Eq. (4.2), are not quite as disfavored. In this case the hierarchies among different mass matrix elements are softer, and one can ask whether the red dots in Fig. 9 can move toward the experimentally allowed regions with order 1–10 relative shifts. Many of the predictions are already in agreement with experimental constraints, or at least close enough to be easily ''nudged'' toward acceptable levels with order one coefficients. The figure reveals that only $m_{\mu\mu}$ is predicted to be relatively too small. By enhancing it by a factor of order $y_\tau/y_\mu \sim 20$, one obtains moderately good agreement between Eq. (4.2) and experimental requirements. We therefore conclude that operators listed in Eq. (4.1) are at least marginally allowed by neutrino mixing phenomenology.

While essential for a complete understanding of neutrino masses and mixing, improved measurements of the already determined mixing angles and mass-squared differences will not help to further constrain/exclude any of the LNV scenarios in question. Considering our parameter flexibility, only future neutrino experiments that provide qualitatively new results can aid in this endeavor. In particular, the experimental determination of the neutrino-mass hierarchy is essential in order to properly test the scenarios highlighted in this section, as they all predict, in the absence of very nontrivial flavor structure in the LNV sector, the normal hierarchy. Next-generation neutrino oscillation experiments are expected to provide nontrivial information regarding the neutrino-mass hierarchy. Most rely on a neutrino/antineutrino oscillation asymmetry via Earth matter effects [1,43], and depend heavily on a sufficiently large θ_{13} mixing angle. The possibility that θ_{13} is vanishingly small, where the standard approach is ineffective, is addressed in [43] considering both oscillation and nonoscillation probes. In that case, one can hope to discern the neutrino-mass spectrum in future neutrino factory [19]/superbeam [18] experiments coupled with improved constraints on the effective masses extracted from tritium beta decay [7] and cosmology [6].[15] Note that these nonoscillation probes can be independently used to constrain LNV models, as they provide information regarding the magnitude of the lightest mass eigenstate [m_1 (m_3) in the case of normal (inverted) hierarchy]. For example, if either cosmological observations or tritium beta-decay experiments see evidence for nonzero neutrino masses (in more detail, they constrain $\Sigma = \sum_i m_i$ and $m^2_{\nu_e} = \sum_i m_i^2 |U_{ei}|^2$, respectively) such that $\Sigma \gg 0.05$ eV or $m_{\nu_e} \gg 0.01$ eV, one would conclude, assuming a normal mass hierarchy, that $m_1 \gg \sqrt{\Delta m^2_{12}}$. This would destroy the possibility of negligibly small m_{ee}, and hence disfavor the operators that lead to mass matrices of the type Eqs. (4.2) and (4.3). Currently, Σ and m_{ν_e} are bounded to be below 0.94 eV and 2.0 eV, respectively, but the sensitivity to these observables is expected to significantly improve with next-generation experiments to 0.1 eV [44] and 0.2 eV [45], respectively.

V. PHENOMENOLOGICALLY INTERESTING OPERATORS: SAMPLE RENORMALIZABLE MODEL

Having superficially surveyed a large set of LNV operators, we are now in a position to identify operators with interesting phenomenological features for further detailed study. One subset of potentially interesting operators is characterized by those that, when required to ''explain'' the observed neutrino masses, are accompanied by a low cutoff scale of, say, less than several TeV. Further requiring a small enough $m^{\rm eff}_{ee}$ in order to evade current $\beta\beta0\nu$ constraints, this set contains only seven elements: $\mathcal{O}_{17}$, $\mathcal{O}_{18}$, $\mathcal{O}_{34}$, $\mathcal{O}_{35}$, $\mathcal{O}_{56}$, $\mathcal{O}_{57}$, $\mathcal{O}_{58}$. Of these, all but operators $\mathcal{O}_{35}$ and $\mathcal{O}_{58}$ [which lead to the zeroth-order neutrino-mass matrix Eq. (4.2) and a suppressed m_{ee}] should provide a positive LNV signal in the next round of double-beta-decay experiments, baring specific flavor symmetries or finely tuned couplings. Furthermore, $\mathcal{O}_{56}$ leads to a $\beta\beta0\nu$ rate that is higher than what is naively dictated by the values of the neutrino masses. Finally, with the possible exception of $\mathcal{O}_{56}$, which may mediate observable LNV processes at high-energy colliders, none of the seven operators above are expected to mediate LNV violating phenomena (as defined here) at accessible rates.

An ''orthogonal'' subset consists of the higher dimensional operators already ''excluded'' by $\beta\beta0\nu$. Not including those operators severely constrained by lepton mixing in Sec. IV, this list contains 11 elements: $\mathcal{O}_{16}$, $\mathcal{O}_{19}$, $\mathcal{O}_{53}$, $\mathcal{O}_{54a,b,c,d}$, $\mathcal{O}_{59}$, $\mathcal{O}_{60}$, $\mathcal{O}_{70}$, $\mathcal{O}_{75}$. Most of these are associated with cutoff scales of order the weak scale, which are likely to already be constrained by different searches for new degrees of freedom with masses around 100 GeV. Even if those are considered to be excluded, $\mathcal{O}_{16}$, $\mathcal{O}_{19}$, $\mathcal{O}_{75}$ are ''safely'' shielded from direct and indirect non-LNV searches,[16] while still mediating potentially observable

[15] One traditionally includes the effective $\beta\beta0\nu$ mass m_{ee} given by Eq. (3.2) in a neutrino-mass hierarchy analysis. However, as discussed in Sec. III A, $m^{\rm eff}_{ee}$ is a potentially convoluted process-dependent quantity that generally has little (directly) to do with neutrino masses. For this reason, $\beta\beta0\nu$ constraints cannot be used to determine the neutrino-mass spectrum from the point of this analysis.

[16] New degrees of freedom at the weak scale are constrained by direct and indirect searches at other high-energy colliders (e.g., resonances and effective four-fermion interactions, respectively), flavor-violating (e.g., $\mu \to e\gamma$), and high-precision experiments (e.g., measurements of the anomalous muon magnetic moment).

LNV effects at colliders as long as the new physics does not couple, to zeroth order, to first generation quarks (in order to evade the $\beta\beta0\nu$ constraints).

Regardless of whether these different options for the LNV sector lead to observable LNV phenomena, the low extracted cutoff scale of *all* the operators highlighted above implies that new degrees of freedom should be produced and, with a little luck, observed at the LHC or, perhaps, the ILC. Furthermore, the TeV scale has already been identified as an interesting candidate scale for new physics for very different reasons, including the dark matter puzzle and the gauge hierarchy problem. The fact that, perhaps, the physics responsible for neutrino masses also "lives" at the TeV scale is rather appealing.

In order to study this new physics, as already emphasized earlier, ultraviolet complete manifestations of the physics that leads to the effective operators are required. Here we discuss one concrete example. Other examples (for different effective operators) were discussed in [2]. Given a specific LNV operator, it is a simple matter to write down equivalent renormalizable Lagrangians. We briefly illustrate this procedure by constructing a renormalizable model that will lead to the dimension-11 operator $\mathcal{O}_{56}$. It is among the interesting LNV effective operators of the sample highlighted above, since it is currently unconstrained by $\beta\beta0\nu$ searches regardless of the quark-flavor structure of the operator, while $m_{ee}^{\rm eff} \gg m_{ee}$ for $\beta\beta0\nu$. On the other hand, Λ_ν for $\mathcal{O}_{56}$ is very low (below 500 GeV), so that the new degrees of freedom may already be constrained by, for example, Tevatron or LEP data. We will not worry about such constraints henceforth, but will only comment on possible phenomenological problems.

$\mathcal{O}_{56}$ can be accommodated by a wide variety of models, as can be seen from its possible Lorentz structures. In terms of scalar/tensor helicity-violating bilinears $\Gamma_\nu = 1, \sigma_{\mu\nu}$, and vector helicity-conserving bilinears $\Gamma_c = \gamma_\mu$, these are

$$\begin{aligned}\mathcal{O}_{56} = \{&(L^i\Gamma_\nu Q^j)(d^c\Gamma_\nu d^c)(\bar{d}^c\Gamma_\nu \bar{e}^c), (L^i\Gamma_\nu Q^j)(d^c\Gamma_c \bar{d}^c)(d^c\Gamma_c \bar{e}^c), (L^i\Gamma_\nu d^c)(Q^j\Gamma_\nu d^c)(\bar{d}^c\Gamma_\nu \bar{e}^c), (L^i\Gamma_\nu d^c)(Q^j\Gamma_c \bar{d}^c)\\ &\times (d^c\Gamma_c \bar{e}^c), (L^i\Gamma_\nu d^c)(Q^j\Gamma_c \bar{e}^c)(d^c\Gamma_c \bar{d}^c), (L^i\Gamma_c \bar{d}^c)(Q^j\Gamma_\nu d^c)(d^c\Gamma_c \bar{e}^c), (L^i\Gamma_c \bar{d}^c)(Q^j\Gamma_c \bar{e}^c)(d^c\Gamma_\nu d^c), (L^i\Gamma_c \bar{e}^c)\\ &\times (Q^j\Gamma_\nu d^c)(d^c\Gamma_c \bar{d}^c), (L^i\Gamma_c \bar{e}^c)(Q^j\Gamma_c \bar{d}^c)(d^c\Gamma_\nu d^c)\} \times H^k H^l \epsilon_{ik}\epsilon_{jl}. \end{aligned} \tag{5.1}$$

It is clear from the chiral field content that these operators depend on a combination of helicity-conserving and helicity-violating interactions. In particular, it is impossible to form any of the operators in this long list with only the addition of vector boson states: new heavy scalar and/or tensor particles are probably required if $\mathcal{O}_{56}$ is the proper tree-level manifestation of the LNV physics at low energies.[17] Furthermore, the couplings of the new physics fields with one another must be constrained in order to "block" the presence of lower dimensional tree-level effective operators. This usually implies the existence of new exact (broken) symmetries to forbid (suppress) particular interactions.

Certain Lorentz structures, those containing only Γ_ν bilinears, can be realized assuming that the LNV ultraviolet sector contains only heavy *scalar* fields and we concentrate, for simplicity, on this possibility [46]. Simple scalar interactions that can lead to $\mathcal{O}_{56}$ are shown in the diagram in Fig. 10. Specifically, these yield the effective operator Lorentz structure $(L^iQ^j)(d^cd^c)(\bar{e}^c\bar{d}^c)H^kH^l\epsilon_{ik}\epsilon_{jl}$ with the introduction of four charged scalar fields, ϕ_1, ϕ_2, ϕ_3, ϕ_4. The gauge structure is such that, under $(SU(3)_c, SU(2)_L, U(1)_Y)$,[18] ϕ_1 transforms as a $(\bar{3}, 3, +1/3)$, ϕ_2 as $(\bar{3}, 1, -2/3)$, ϕ_3 as $(3, 1, -4/3)$, and ϕ_4 as $(\bar{3}, 1, -2/3)$. While ϕ_2 and ϕ_4 have identical gauge quantum numbers, they have different baryon number ($2/3$ versus $-1/3$). ϕ_1 has baryon number $-1/3$, while ϕ_3 has baryon number $1/3$. Lepton number cannot be consistently assigned as it is explicitly violated by two units.

ϕ_4, which does not couple to any of the SM fermions, plays an essential role. It acts as a selective "insulator" that connects the various interaction terms in such a way as to only allow certain tree-level higher dimensional SM effective operators. All renormalizable theories that lead to only very high dimensional effective operators contain one or more of these "hidden sector" fields. Note that the new scalar fields should not acquire vacuum expectation values in order to avoid the presence of lower dimensional irrelevant operators that are likely to dominate low-energy phenomenology and—much more importantly—to prevent the spontaneous breaking of color or electromagnetic charge.

Given the scalar field content as well as its transformation properties under SM global and local symmetries, it is a simple matter to write down the minimal interaction Lagrangian density for the system. A candidate renormalizable Lagrangian is

$$\begin{aligned}\mathcal{L} = \mathcal{L}^{(\rm SM)} &+ \sum_i (|D_\mu \phi_I|^2 + M_i|\phi_i|^2) + y_1 QL\phi_1\\ &+ y_2 d^c d^c \phi_2 + y_3 e^c d^c \phi_3 + \lambda_{14}\bar{\phi}_1\phi_4 HH\\ &+ \lambda_{234} M \phi_2 \bar{\phi}_3 \phi_4 + \text{H.c.}\end{aligned} \tag{5.2}$$

Each term in Eq. (5.2), including those involving covariant

[17] Other possibilities include heavy vectorlike fermions.

[18] In the case of $U(1)_Y$, "transfoms as X" means "has hypercharge X."

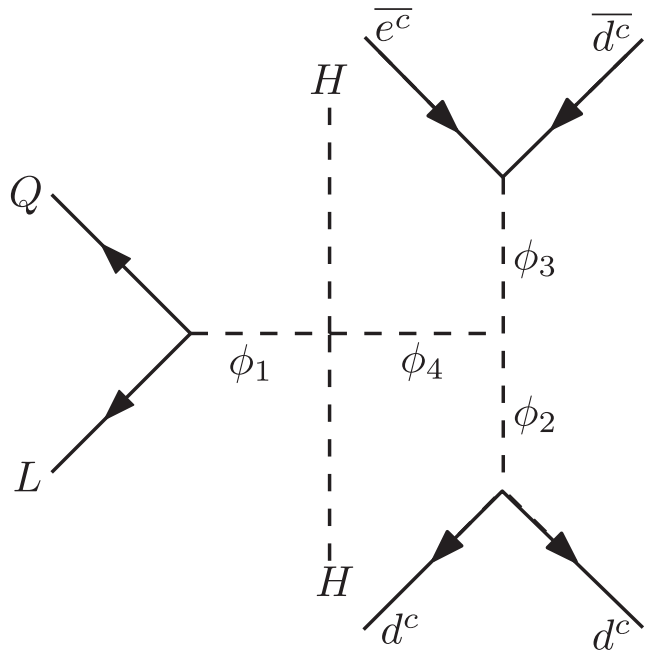

FIG. 10. Sample scalar interactions that lead to the interesting effective operator $\mathcal{O}_{56}$ with the Lorentz structure $(L^i Q^j)(d^c d^c) \times (\bar{e}^c \bar{d}^c) H^k H^l \epsilon_{ik} \epsilon_{jl}$.

derivatives D_μ, is implicitly assumed to respect the gauge representations of the associated ϕ_i fields, as defined above. The Yukawa-type couplings y_i, as well as the λ_i scalar vertices are dimensionless, and assumed to be of order one, while we assume all scalar masses M_i to be of the same order of magnitude. In this case, $\Lambda \sim M_i$. In the λ_{234} term, an overall mass scale M has been "factored out" and is assumed to be of the same order as the M_i. Note that we neglect generation indices, which are implied. In the case $\lambda_{234} = 0$, lepton number is a classical global symmetry of Eq. (5.2), and one can view this three-scalar coupling as the source of lepton number violation. One may even envision a scenario where lepton number is spontaneously broken by the vacuum expectation value of some SM singlet ϕ_5 scalar field, $\langle \phi_5 \rangle = M$.

Provided all M_i are around 0.5 TeV, as required if this Lagrangian is to explain the observed light neutrino masses, LNV is certainly *not* the only (or even the main) consequence of this model. The y_1 and y_3 terms, for example, will mediate $\mu \to e$ conversion in nuclei at very dangerous levels if their flavor structure is generic. ϕ_2 can be resonantly produced in dd collisions, while ϕ_1 and ϕ_3 qualify as scalar lepto-quarks, which are constrained by high-energy collider experiments, including those at HERA [47], to weigh more than a few hundred GeV [17]. For more details, we refer readers to, for example, the Particle Data Book [17] and references therein.

We will conclude this discussion by adding that several other effective operators can be realized in a very similar way. $\mathcal{O}_{19}$, for example, if it manifests itself with the Lorentz structure $(L^i Q^j)(d^c d^c)(\bar{e}^c \bar{u}^c)\epsilon_{ij}$, can be realized by a Lagrangian very similar to Eq. (5.2) where the d^c field in the y_3-coupling interaction is replaced by a u^c field, and the ϕ_1 field is replaced by an $SU(2)_L$ singlet [it is a triplet in Eq. (5.2)]. Of course, hypercharge assignments for the ϕ_i also need to be modified in a straightforward way. The associated non-LNV phenomenology is similar, except for the fact that Λ_ν for $\mathcal{O}_{19}$ (around 1 TeV) is larger than the one for $\mathcal{O}_{56}$ and hence $\mathcal{O}_{19}$ is less constrained by current experimental data. On the other hand, $\mathcal{O}_{19}$ predicts potentially much larger rates for LNV observables at colliders (see Fig. 7).

Our definition of interesting is arbitrary and motivated only by the fact that the physics of the interesting operators highlighted earlier in this section will probably be explored at next-generation collider and high-precision experiments. One may argue that many operators which lead to the observable neutrino masses for high values of Λ_ν are interesting in their own right, either due to the theoretically pleasing properties of their associated potential ultraviolet completions, or by some observational peculiarity. There are many examples of the first type, ranging from the different manifestations of the seesaw mechanism [9–12] to the Zee model [48] and the minimal supersymmetric SM with R-parity violation [49]. Dedicated analyses of these cases have been widely pursued in the literature and will not be discussed here. We would also like to point out that some effective operators, like $\mathcal{O}_7$ and $\mathcal{O}_8$, are, according to our criteria, very "uninteresting." Both $\mathcal{O}_7$ and $\mathcal{O}_8$ predict unobservably suppressed $\beta\beta0\nu$ rates (both predict small m_{ee}) and equally hopeless collider prospects given that they are associated with very high cutoff scales, $\Lambda_\nu \approx 4 \times 10^2$ TeV and $\Lambda_\nu \approx 6 \times 10^3$ TeV, respectively. If either of these operators is responsible for the observed tiny neutrino masses, it is quite possible that we may never directly detect LNV. It is curious to consider possible means of indirect detection or other observable consequences of the different ultraviolet completions of such scenarios.[19] It would also be interesting to ask whether either of these elusive models has any underlying theoretical motivation or whether they allow one to solve other outstanding problems in particle physics.

VI. DISCUSSION AND CONCLUDING REMARKS

If neutrino masses are a consequence of lepton number violating physics at a very high-energy scale (higher than the scale of electroweak symmetry breaking), new physics effects—including the generation of neutrino Majorana masses—at low enough energies can be parametrized in terms of irrelevant operators whose coefficients are sup-

[19]This is very similar to the case of $\mathcal{O}_1$. The main redeeming feature of $\mathcal{O}_1$, other than its simplicity, is the fact that many of its ultraviolet completions allow one to explain the matter-antimatter asymmetry of the universe [13].

pressed by inverse powers of an effective cutoff scale Λ. As discussed before, Λ is, roughly, the energy scale above which new degrees of freedom must be observed if the new ultraviolet physics is perturbative (if the new physics is very weakly coupled, the masses of the new degrees of freedom can be much smaller than Λ). We have explored a very large class of such scenarios through 129 irrelevant operators of energy dimension less than or equal to 11 that violate lepton number by 2 units. These are tabulated in the first two columns of Table I, along with a summary of our results.

Analyzing each effective operator individually, we estimated the predicted general form of the Majorana neutrino-mass matrix. Our results are listed in the third column of Table I. By comparing each such estimate with our current understanding of neutrino masses, we extracted the cutoff scale Λ_ν of each effective operator, assuming that it provides the dominant contribution to the observed neutrino masses. These results are listed in the fourth column of Table I assuming light neutrino masses equal to 0.05 eV (the square root of the atmospheric mass-squared difference), and are summarized as follows. Depending on the field content and dimension of the irrelevant operator, the ''lepton number breaking scale'' Λ_ν is predicted to be anywhere from the weak scale (~ 0.1 TeV) all the way up to 10^{12} TeV (see Fig. 2). This means that, depending on how lepton number is violated and communicated to the SM, the mass of the associated new degrees of freedom is predicted to be anywhere between 100 GeV and 10^{12} TeV, *even if all new physics couplings are order one*. We note that, in the case of all variations of the seesaw mechanism ($\mathcal{O}_1$), neutrino physics constrains $\Lambda_\nu = 10^{12}$ TeV such that the new degrees of freedom are either unobservably heavy, extremely weakly coupled, or their couplings to the SM degrees of freedom are finely tuned. It is fair to say that this behavior is not characteristic of all LNV ultraviolet physics. One sample ultraviolet theory that leads to dimension-11 LNV effective operators was discussed in Sec. V. Other examples can be found in [2], and include supersymmetry with trilinear R-parity violation and the Zee model.

Assuming that a particular operator is responsible for nonzero neutrino masses, it is straightforward to ask whether it leads to other observable consequences. Here, we concentrated on several LNV observables, and included future LNV searches at the LHC and future lepton machines (like the ILC), along with their ability to directly produce (and hopefully observe) new physics states lighter than several hundred GeV. In column five of Table I, we list the most favorable modes of experimental observation for each operator. The different relevant probes are neutrinoless double-beta decay ($\beta\beta0\nu$), neutrino oscillation and mixing (mix), direct searches for new particles at the LHC (LHC) and ILC (ILC), and virtual LNV effects at collider facilities (HElnv). We find it unlikely that other probes of LNV, including rare meson decays, should yield a positive signal in the forseeable future. This conclusion is strongly based on the fact that, for all of our analysis, we assume that *all* new physics degrees of freedom are heavier than the weak scale. While the vast majority of operators is most sensitive to searches for neutrinoless double-beta decay, that is not true of all operators. Some lead to relatively suppressed rates for $\beta\beta0\nu$ (mostly because they lead to mass matrices with a very small m_{ee}) even if they are associated with $\Lambda_\nu < 1$ TeV, indicating that, for these scenarios, we are more likely to observe the physics behind neutrino masses directly at colliders than to see a finite lifetime for $\beta\beta0\nu$. Other scenarios naively lead to $\beta\beta0\nu$ rates orders of magnitude higher than what is currently allowed by data. If these are responsible for the generation of neutrino masses, the new physics is constrained to be somewhat decoupled from first generation quarks (for example). In this case, there is hope that LNV phenomena at colliders, which are not restricted to first generation quarks, occur with non-negligible rates.

The sixth column of Table I lists the current ''status'' of the operator as either experimentally unconstrained (U), constrained (C), or disfavored (D). Such labels are assigned based only on the experimental probes reviewed in this work. By arbitrary convention, an ''unconstrained'' operator can safely accommodate all existing data even if one assumes *all* its flavor-dependent dimensionless coefficients to be of order one. A ''constrained'' operator can accommodate all existing data after one allows some of the different flavor-dependent dimensionless coefficients to be suppressed with respect to the dominant ones by a factor of 100 or so (as described above). ''Disfavored'' operators can only accommodate all data if ''tuned'' much more severely than the constrained ones, and are usually in trouble with more than one ''type'' of constraint. A glance at column six reveals that 11 out of the 129 operators are disfavored by current data. The most stringent constraints come from $\beta\beta0\nu$, while all disfavored operators are associated with cutoffs at or below 1 TeV. Three of the disfavored operators, $\mathcal{O}_{36}$, $\mathcal{O}_{37}$, and $\mathcal{O}_{38}$, are also in disagreement with the neutrino oscillation data (see Sec. IV).

Our results illustrate that, as far as ''explaining'' neutrino masses, the model-building scene is wide open even if one postulates that neutrino masses arise as a consequence of lepton number violating, ''heavy'' physics. Significant progress will only be achieved once more experimental information becomes available. The observation that neutrinoless double-beta decay occurs with a nonzero rate will help point us in the right direction, but will certainly not reveal much about the mechanism behind neutrino masses. A more complete picture can only arise from combined information from several observables, including other LNV observables and the search for new physics at the electroweak scale. Other important experimental searches,

not discussed here, include all lepton number conserving leptonic probes, such as precision measurements of the anomalous magnetic moment of the muon, searches for leptonic electric dipole moments, searches for charged-lepton flavor violation (see [50] for a model-independent discussion of this issue), and precision measurements of neutrino–nucleon and neutrino–lepton scattering.

ACKNOWLEDGMENTS

J. J. would like to thank Michael Schmitt for useful insight into the experimental feasibility of some of these analyses, as well as the members of the Argonne National Laboratory theory group for help in identifying limitations to our assumed operator set. A. d. G. is indebted to Kai Zuber for discussions on the relevance of probes of lepton number violation besides $\beta\beta0\nu$. This work is sponsored in part by the U.S. Department of Energy Contract No. DE-FG02-91ER40684.

[1] See, for example, M. C. Gonzalez-Garcia and M. Maltoni, arXiv:0704.1800; A. Strumia and F. Vissani, arXiv:hep-ph/0606054; R. N. Mohapatra *et al.*, Rep. Prog. Phys. **70**, 1757 (2007); A. de Gouvêa, Mod. Phys. Lett. A **19**, 2799 (2004); arXiv:hep-ph/0411274.

[2] K. S. Babu and C. N. Leung, Nucl. Phys. **B619**, 667 (2001).

[3] M. Maltoni, T. Schwetz, M. A. Tortola, and J. W. F. Valle, New J. Phys. **6**, 122 (2004).

[4] C. Kraus *et al.*, Eur. Phys. J. C **40**, 447 (2005).

[5] V. M. Lobashev *et al.*, Nucl. Phys. B, Proc. Suppl. **91**, 280 (2001).

[6] For recent estimates see G. L. Fogli *et al.*, Phys. Rev. D **75**, 053001 (2007); S. Hannestad and G. G. Raffelt, J. Cosmol. Astropart. Phys. 11 (2006) 016; U. Seljak, A. Slosar, and P. McDonald, J. Cosmol. Astropart. Phys. 10 (2006) 014. For a recent comprehensive review, see J. Lesgourgues and S. Pastor, Phys. Rep. **429**, 307 (2006).

[7] For a recent detailed discussion, see Y. Farzan and A. Yu. Smirnov, Phys. Lett. B **557**, 224 (2003).

[8] L. J. Hall, H. Murayama, and N. Weiner, Phys. Rev. Lett. **84**, 2572 (2000); A. de Gouvêa and H. Murayama, Phys. Lett. B **573**, 94 (2003).

[9] P. Minkowiski, Phys. Lett. **67B**, 421 (1977); M. Gell-Mann, P. Ramond, and R. Slansky, in *Supergravity*, edited by D. Freedman and P. Van Niuenhuizen (North Holland, Amsterdam, 1979), p. 315; T. Yanagida, in *Proceedings of the Workshop on Unified Theory and Baryon Number in the Universe*, edited by O. Sawada and A. Sugamoto (KEK, Tsukuba, Japan, 1979); S. L. Glashow, *1979 Cargèse Lectures in Physics—Quarks and Leptons*, edited by M. Lévy *et al.* (Plenum, New York, 1980), p. 707. See also R. N. Mohapatra and G. Senjanović, Phys. Rev. Lett. **44**, 912 (1980); J. Schechter and J. W. F. Valle, Phys. Rev. D **22**, 2227 (1980).

[10] E. Ma, Phys. Rev. Lett. **81**, 1171 (1998); B. Bajc and G. Senjanovic, J. High Energy Phys. 08 (2007) 014.

[11] R. N. Mohapatra and G. Senjanovic, Phys. Rev. D **23**, 165 (1981); G. B. Gelmini and M. Roncadelli, Phys. Lett. **99B**, 411 (1981).

[12] R. Foot, H. Lew, X. G. He, and G. C. Joshi, Z. Phys. C **44**, 441 (1989).

[13] M. Fukugita and T. Yanagida, Phys. Lett. B **174**, 45 (1986). For a recent review, see W. Buchmuller, R. D. Peccei, and T. Yanagida, Annu. Rev. Nucl. Part. Sci. **55**, 311 (2005).

[14] A. Pilaftsis, Z. Phys. C **55**, 275 (1992); J. Bernabéu, A. Santamaria, J. Vidal, A. Mendez, and J. W. F. Valle, Phys. Lett. B **187**, 303 (1987); W. Buchmuller and D. Wyler, Phys. Lett. B **249**, 458 (1990); W. Buchmuller and C. Greub, Nucl. Phys. **B363**, 345 (1991); A. Datta and A. Pilaftsis, Phys. Lett. B **278**, 162 (1992); G. Ingelman and J. Rathsman, Z. Phys. C **60**, 243 (1993); C. A. Heusch and P. Minkowski, Nucl. Phys. **B416**, 3 (1994). For recent discussions, see J. Kersten and A. Yu. Smirnov, Phys. Rev. D **76**, 073005 (2007); A. de Gouvêa, arXiv:0706.1732.

[15] A. de Gouvêa, J. Jenkins, and N. Vasudevan, Phys. Rev. D **75**, 013003 (2007); A. de Gouvêa, Phys. Rev. D **72**, 033005 (2005); T. Asaka, S. Blanchet, and M. Shaposhnikov, Phys. Lett. B **631**, 151 (2005); D. Gorbunov and M. Shaposhnikov, J. High Energy Phys. 10 (2007) 015.

[16] A. Atre, V. Barger, and T. Han, Phys. Rev. D **71**, 113014 (2005).

[17] W. M. Yao *et al.* (Particle Data Group), J. Phys. G **33**, 1 (2006).

[18] W. T. Weng *et al.*, J. Phys. G **29**, 1735 (2003); Y. Oyama, arXiv:hep-ex/0512041; M. G. Albrow *et al.*, arXiv:hep-ex/0509019.

[19] See, for example, C. H. Albright *et al.* (Neutrino Factory/Muon Collider Collaboration), arXiv:physics/0411123; S. Geer, Phys. Rev. D **57**, 6989 (1998); **59**, 039903 (1999).

[20] P. Zucchelli, Phys. Lett. B **532**, 166 (2002).

[21] J. Maalampi and N. Romanenko, Phys. Lett. B **474**, 347 (2000).

[22] See, for example, S. R. Elliott and P. Vogel, Annu. Rev. Nucl. Part. Sci. **52**, 115 (2002); M. Doi, T. Kotani, and E. Takasugi, Prog. Theor. Phys. Suppl. **83**, 1 (1985); A. S. Barabash, JINST **1**, P07002 (2006).

[23] For a recent assessment, see V. A. Rodin, A. Faessler, F. Simkovic, and P. Vogel, Nucl. Phys. **A766**, 107 (2006); Nucl. Phys. **A766**, 107 (2006); **A793**, 213(E) (2007).

[24] H. V. Klapdor-Kleingrothaus, I. V. Krivosheina, A. Dietz, and O. Chkvorets, Phys. Lett. B **586**, 198 (2004).

[25] H. V. Klapdor-Kleingrothaus *et al.*, Eur. Phys. J. A **12**, 147 (2001).

[26] C. E. Aalseth *et al.* (IGEX Collaboration), Phys. Rev. D **65**, 092007 (2002).

[27] S. M. Bilenky, C. Giunti, J. A. Grifols, and E. Masso, Phys. Rep. **379**, 69 (2003); C. Aalseth *et al.*, arXiv:hep-ph/0412300.

[28] M. Flanz, W. Rodejohann, and K. Zuber, Phys. Lett. B **473**, 324 (2000); **480**, 418 (2000).

[29] A. G. Akeroyd *et al.* (SuperKEKB Physics Working Group), arXiv:hep-ex/0406071; I. I. Bigi and A. I. Sanda, arXiv:hep-ph/0401003.

[30] See, for example, J. Drees, Int. J. Mod. Phys. A **17**, 3259 (2002).

[31] See, for example, M. Breidenbach, IEEE Trans. Nucl. Sci. **33**, 46 (1986).

[32] A. Abbaneo *et al.* (LEP Collaboration, ALEPH Collaboration, DELPHI Collaboration, L3 Collaboration, OPAL Collaboration, LEP Electroweak Working Group, SLD Electroweak Group, and SLD Heavy Flavor Group), arXiv:hep-ex/0312023; see also M. Carena, A. de Gouvêa, A. Freitas, and M. Schmitt, Phys. Rev. D **68**, 113007 (2003).

[33] S. Bar-Shalom, N. G. Deshpande, G. Eilam, J. Jiang, and A. Soni, Phys. Lett. B **643**, 342 (2006).

[34] See, for example, G. Rolandi, Int. J. Mod. Phys. A **21**, 1654 (2006).

[35] See, for example, M. Alabau Pons, P. Bambade, O. Dadoun, R. Appleby, and A. Faus-Golfe, arXiv:physics/0609043; R. D. Heuer, Nucl. Phys. B, Proc. Suppl. **154**, 131 (2006). See also http://www.linearcollider.org/cms/.

[36] D. London, G. Belanger, and J. N. Ng, Phys. Lett. B **188**, 155 (1987).

[37] K. Moffeit, M. Woods, P. Schuler, K. Moenig, and P. Bambade, Report No. SLAC-TN-05-045, No. LCC-0159, and No. IPBI-TN-2005-2.

[38] C. M. Ankenbrandt *et al.*, Phys. Rev. ST Accel. Beams **2**, 081001 (1999); M. M. Alsharoa *et al.* (Muon Collider/Neutrino Factory Collaboration), Phys. Rev. ST Accel. Beams **6**, 081001 (2003). See also http://www.fnal.gov/projects/muon_collider/.

[39] See, for example, V. I. Telnov, Acta Phys. Pol. B **37**, 1049 (2006); E. Accomando *et al.* (CLIC Physics Working Group), arXiv:hep-ph/0412251.

[40] See, for example, F. del Aguila, J. A. Aguilar-Saavedra, and R. Pittau, J. High Energy Phys. 10 (2007) 047; A. Datta, M. Guchait, and A. Pilaftsis, Phys. Rev. D **50**, 3195 (1994); F. M. L. de Almeida, Y. D. A. Coutinho, J. A. Martins Simões, A. J. Ramalho, S. Wulck, and M. A. B. do Vale, Phys. Rev. D **75**, 075002 (2007); T. Han and B. Zhang, Phys. Rev. Lett. **97**, 171804 (2006); O. Panella, M. Cannoni, C. Carimalo, and Y. N. Srivastava, Phys. Rev. D **65**, 035005 (2002); A. Ali, A. V. Borisov, and N. B. Zamorin, Eur. Phys. J. C **21**, 123 (2001); arXiv:hep-ph/0112043.

[41] M. Frigerio and A. Yu. Smirnov, Phys. Rev. D **67**, 013007 (2003); Nucl. Phys. **B640**, 233 (2002); A. Merle and W. Rodejohann, Phys. Rev. D **73**, 073012 (2006).

[42] See, for example, S. M. Bilenky, C. Giunti, C. W. Kim, and S. T. Petcov, Phys. Rev. D **54**, 4432 (1996).

[43] A. de Gouvêa and W. Winter, Phys. Rev. D **73**, 033003 (2006); A. de Gouvêa and J. Jenkins, arXiv:hep-ph/0507021; A. de Gouvêa, J. Jenkins, and B. Kayser, Phys. Rev. D **71**, 113009 (2005).

[44] See, for example, J. Lesgourgues and S. Pastor, in [6]; K. N. Abazajian and S. Dodelson, Phys. Rev. Lett. **91**, 041301 (2003).

[45] A. Osipowicz *et al.* (KATRIN Collaboration), arXiv:hep-ex/0109033. See also http://www-ik.fzk.de/katrin/index.html.

[46] For a scenario that also pursues lepton number violation from new exotic scalar fields, see G. K. Leontaris, K. Tamvakis, and J. D. Vergados, Phys. Lett. **162B**, 153 (1985).

[47] See, for example, C. Adloff *et al.* (H1 Collaboration), Eur. Phys. J. C **11**, 447 (1999); **14**, 255 (2000).

[48] A. Zee, Nucl. Phys. **B264**, 99 (1986).

[49] For overviews, see R. Barbier *et al.*, Phys. Rep. **420**, 1 (2005); H. K. Dreiner, arXiv:hep-ph/9707435.

[50] D. Black, T. Han, H. J. He, and M. Sher, Phys. Rev. D **66**, 053002 (2002).